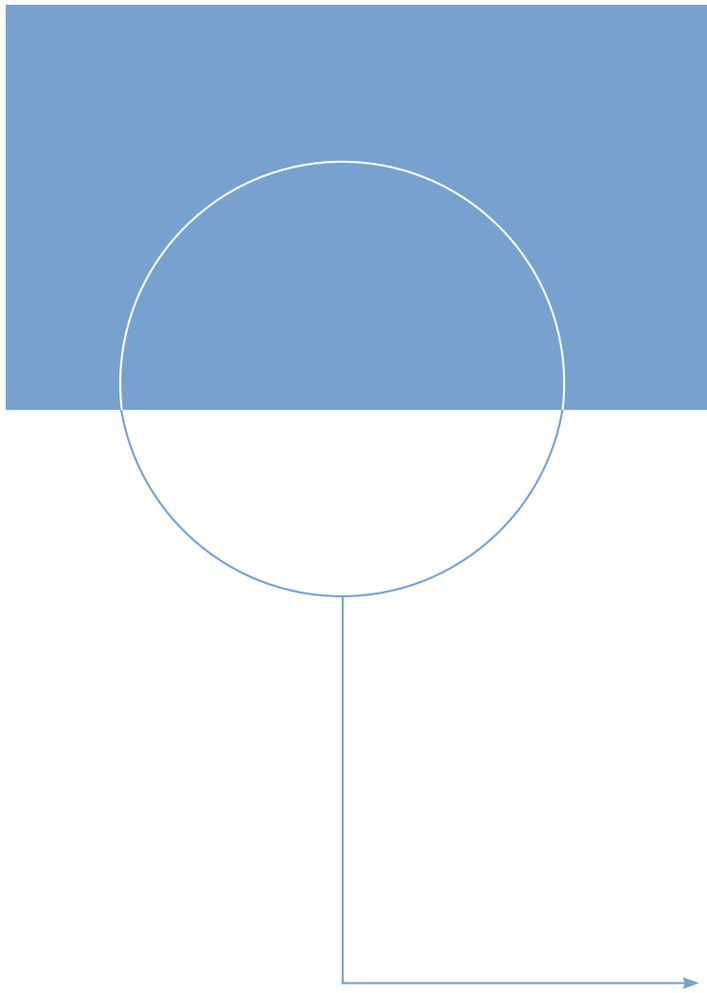

Master's thesis

2019

Mathias Finanger Øverdal

NTNU
Norwegian University of
Science and Technology
Faculty of Natural Sciences
Department of Physics

Mathias Finanger Øverdal

Optimization of diffusion weighted-MRI: a study of T2 and ADC in healthy fibroglandular breast tissue

June 2019

NTNU
Norwegian University of
Science and Technology

NTNU
Norwegian University of
Science and Technology

NTNU

Norwegian University of
Science and Technology

Optimization of diffusion weighted-MRI: a study of T2 and ADC in healthy fibroglandular breast tissue

Mathias Finanger Øverdal

MLREAL
Submission date: June 2019
Supervisor: Pål Erik Goa

Norwegian University of Science and Technology
Department of Physics

Abstract

Diffusion weighted-magnetic resonance imaging (DW-MRI) is becoming increasingly more popular for detecting, staging and evaluating response to treatment in breast cancers. The apparent diffusion coefficient (ADC) is largely reduced in malignant lesions and DW-MRI provides a novel insight of the microstructure. Even though the method is well established and widely used in a clinical setting the detailed relationship between microstructure and the physical mechanisms governing diffusion properties like the ADC are still under debate. The aim of this thesis is to evaluate the effect of diffusion weighting (b) on the spin-spin relaxation (T2) and the effect of echo time (TE) on the measured ADC for the optimization of protocol parameters in DW-MRI. T2 and ADC are measured in the healthy fibroglandular tissue of three female volunteers. The measured ADC was found to decrease for prolonged TE while T2 was found to increase with b-value. An attempt to explain the dependency of TE on ADC and b on T2 was made and evaluated using two different biophysical models of breast tissue.

Sammendrag

Diffusjonsvektet magnetisk resonansavbildning er blitt stadig mer populært i deteksjon, gradering og evaluering av respons på behandling i brystkreft. Den tilsynelatende diffusjonskonstanten (ADC) reduseres i stor grad i ondartede svulster og diffusjonsvektet avbildning gir ny innsikt i mikrostruktur. Selv om metoden er veletablert og mye brukt i klinisk setting, er det detaljerte forholdet mellom mikrostruktur og de fysiske mekanismene som styrer ADC fortsatt debattert. Formålet med denne oppgaven er å evaluere effekten av diffusjonsvekting (b) på T2 og effekten av ekkotid på ADC for optimalisering av parametetere i diffusjonsvektet magnetisk resonansavbildning. T2 og ADC er målt i friskt fibroglandulært brystvev hos tre friske frivillige. Målt ADC ble funnet til å minke for økt ekkotid, mens T2 blir målt til å stige for økt b-verdi. Avhengigheten av ekkotid på ADC og b på T2 ble målt og evaluert ved hjelp av to biofysiske modeller av brystvev.

Acknowledgements

This thesis is the final part of my masters degree and marks the end of five wonderful years at the Norwegian University of Science and Technology, NTNU. First I would like to thank my supervisor, Associate professor Pål Erik Goa for guidance, help and support through both the specialization project in physics that lead to this thesis and the entire master work itself.

As I will soon leave NTNU behind there are numerous things to be grateful for, the friendships and the experiences I have made along the way. The social, cultural and professional rewards of being a student in Trondheim is beyond compare.

I would also like to thank my parents, my sister Martine and my supportive and loving fiancée Karina for always keeping my spirits up.

Mathias Øverdal
Trondheim, June, 2019.

Contents

Abbreviations

ADC	=	Apparent diffusion coefficient
DW	=	Diffusion weighted
DWI	=	Diffusion weighted image
DW-MRI	=	Diffusion weighted-magnetic resonance imaging
EPI	=	Echo planar imaging
FGT	=	Fibroglandular breast tissue
FID	=	Free induction decay
GRE	=	Gradient echo
HES	=	Hematoxylin-eosin-saffron
MR	=	Magnetic resonance
MRI	=	Magnetic resonance imaging
RF	=	Radio frequency (pulse)
ROI	=	Region of interest
SD	=	Standard deviation
SE	=	Spin echo
TE	=	Echo time
TR	=	Repetition time

Chapter 1

Introduction

Diffusion weighted-magnetic resonance imaging (DW-MRI) is a powerful tool for probing microstructural and physiological properties of cancerous and healthy tissue in vivo at the cellular and subcellular level. This is due to the unique sensitivity of proton magnetic resonance signals to the molecular self diffusion of water at microscopic length scales [1].

Noninvasive cancer imaging biomarkers are important tools for the identification and characterization of neoplastic lesions in vivo, as well as for monitoring tumor response to treatment. Two important biomarkers for cancer detection in MRI is transverse relaxation time, T2 and the apparent diffusion coefficient, ADC. The relationship between signal and these two biomarkers and their relation to each other is non-trivial. The motivation for this research is to create a better understanding of the underlying physical mechanisms behind diffusion in vivo and the sensitivity of the MR-signal on the microstructure - in addition to the dependency of different diffusion times on the estimation of ADC.

The objectives of this thesis is to evaluate the dependency of diffusion weighting on observed T2 found in a previous project. As well as optimization of protocol parameters for future studies and exploration of two possible biophysical models to explain observed signal behaviour in DW-MRI. In vivo data from three healthy volunteers are used in this study for estimation of T2 and ADC in the specific case of healthy fibroglandular breast tissue. The effect of diffusion weighting b on T2 and echo time TE on ADC is evaluated.

Chapter 2

Theory

One of the many advantages with magnetic resonance imaging (MRI) is that it allows for non-invasive probing of biological tissue. Without the use of X-rays or other ionizing radiation, MRI is an imaging technique widely used in medicine to form pictures of anatomy and pathology in the body. Among the original reasons for the excitement about MRI was, and continues to be, its relative safety, where the non-invasive nature of the magnetic fields deployed make it possible to diagnose conditions of people of almost any age [2]. The technique is a form of nuclear magnetic resonance (NMR) and was originally abbreviated NMRI, the term 'nuclear' was removed due to negative associations. 'Magnetic' refers to the magnetic field required to excite the spins of protons, and 'resonance' refers to the need to match the (radio)frequency of an oscillating magnetic field to the precessional frequency of the protons in the tissue [2]. The study and development of modern MRI has provided a highly versatile imaging technique capable of extracting a variety of chemical and physical data.

Some of the following theory is an adaptation of a previously written specialization project written by the author of this thesis.

2.1 Origin of magnetic resonance imaging

Felix Bloch and Edward Purcel discovered independently of each other the phenomenon of magnetic resonance (MR) in 1946. They shared the Nobel Prize in physics for their development of new methods for nuclear magnetic precession measurements and discoveries in connection therewith in 1952. *Spin echo* and the observable signal from MR, *FID*, short for free induction decay was discovered by Erwin Hahn in 1950 [3, 4]. During the sixties and seventies a great number of experiments were made on *relaxation times*. Many scientists from different branches of science have partaken in the development of MRI. The american chemist Paul Lauterbur shared the Nobel Prize with Peter Mansfield in 2003 for their work on spatial encoding and their contribution to the development of MRI. It was already known that a proton would precess under the influence of a magnetic field with a known frequency ω_0. The *Larmor frequency*, dependent only on the magnitude of the magnetic field and the gyromagnetic ratio of protons is given by the simple relation

$$\omega_0 = \gamma B. \tag{2.1}$$

The constant γ is the gyromagnetic ratio - a constant specific to the nucleus, the proton (in water) has a gyromagnetic ratio of approximately 2.68×10^8 rad/s/Tesla [5] and B is the strength of the magnetic field, typically 1.5 or 3 T for clinical scanners.
Lauterbur and Mansfield suggested that if a spatially varying field were to be introduced across the object, then the Larmor frequency would also be spatially dependent. They suggested that the different frequency components could be separated, thus giving spatial information on the examined object [6, 7]. This key point opened the door to imaging with MR, focus on tumor detection was pointed out early on by Damadian [2].

2.2 Relaxation physics

MRI is based on the interaction of nuclear spins with an external field $\vec{B}_0$ and primarily refers to the signal detection of protons. For a proton with only two quantum eigenstates the only two possible alignments are parallel (lower energy) or anti-parallel (higher energy) to the external magnetic field $\vec{B}_0$. The frequency in the quantum energy difference is $\hbar\omega_0$ where $\hbar = h/2\pi = 1.05\times10^{-34}$ m^{2}kg/s, the reduced Planck constant h. The extreme smallness of the quantum spin energy compared to thermal energy means that the fraction $\hbar\omega_0/kT \ll 1$, where $k = 1.38\times10^{-23}$ m^{2}kg/s^{2}K, is Boltzmanns constant and T is absolute temperature. The Boltzmann distribution shows that the number of spins parallel to the field compared to anti-parallel is very small due to high thermal

energy compared to $\hbar\omega_0$, the spin excess is approximately

$$\text{spin excess} \simeq N\frac{\hbar\omega_0}{2kT}, \tag{2.2}$$

where N is the total number of spins. The spin excess is only about 10 in a million spins at a field of 3 T, assuming body temperature of 310 K, however due to the Avogadro numbers of water molecules and even larger number of protons in tissue there is more than enough to generate a good signal.

A single proton in a magnetic field is in a superposition of the two energy eigenstates up (parallel) or down (anti-parallel) and separated by a small energy difference, the *Zeeman* effect. When a single spin is measured the wavefunction which is a linear combination of the parallel and anti-parallel states collapses and can only have one of two results, up or down. The magnetic dipole moment $\vec{\mu}$ of a proton is a quantum superposition state and behaves much like a compass needle in earths magnetic field. The moment $\vec{\mu}$ will seek to align with $\vec{B}_0$ and experiences a torque τ given by the vector cross product $\tau = \mu \times \vec{B}_0$. If one were to take the sum of all dipole moments $\Sigma\mu_i$ the resulting net magnetization is commonly denoted by $\vec{M}$ and behaves in a classical manner. The classical motion of the net magnetisation for an ensemble of spins in the presence of $\vec{B}_0$ is described by the Bloch equation:

$$\frac{d\vec{M}}{dt} = \gamma\vec{M} \times \vec{B}_0. \tag{2.3}$$

By definition, precession is the circular motion of the axis of rotation of a spinning body about another fixed axis, caused by the application of a torque in the direction of the precession [2], see Figure 2.1, this movement is the solution to the Bloch equation (2.3) shown for a single spin, for clarity. The rotating motion of $\vec{M}$ is the basis of the MR signal. The measured signal in an MRI scan is the phase and amplitude of $\vec{M}$ recorded by detecting induced voltage in a receiver coil.

Suppose a static magnetic field $\vec{B}_0 = B_0\hat{z}$ the magnetization vector $\vec{M}$ can be described in parallel and perpendicular components

$$\vec{M}_{\parallel} = M_z, \tag{2.4}$$

and the perpendicular components are

$$\vec{M}_{xy} = M_x\hat{x} + M_y\hat{y}. \tag{2.5}$$

The equations of motion for parallel and perpendicular components of non-interacting

spins are described by equations (2.6) and (2.7).

$$\frac{dM_z}{dt} = 0, \tag{2.6}$$

$$\frac{dM_{xy}}{dt} = \gamma \vec{M}_{xy} \times \vec{B}_0. \tag{2.7}$$

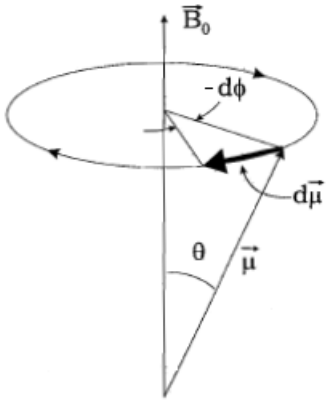

Figure 2.1: The interaction of the protons spin with the magnetic field produces the torque, causing it to precess about $\vec{B}_0$ as the fixed axis. The precession of the magnetic moment vector $\vec{\mu}$ which is proportional to the spin vector, is clockwise. The customary counterclockwise definition of polar angles causes the differential $d\phi$ to be shown negative.

In the rotating frame of reference a typical MRI scan starts with a 90° radio frequency (RF) pulse that tilts the magnetization vector into the plane whose normal is in the direction of the main magnetic field [5]. The RF pulse need to match the Larmor frequency given by (2.1) of the spin ensemble to perturb the magnetization vector. We call the equilibrium value of the magnetization M, M_0. M_{xy} is the distribution of up and down state-spins tilted away from $\vec{B}_0$ and rotating around it. By convention the main magnetic field $\vec{B}_0$ is in the z-direction, horizontal and along the length of the patient being scanned.

2.2.1 T1, T2 and T2* relaxation

After the initial 90° (or any arbitrary non-zero angle) flip of the spins into the transversal plane each spin will seek to regain the initial longitudinal orientation - low energy alignment of the field. That is the reason why T1 relaxation also goes by the name longitudinal relaxation, which is the same. T1 relaxation is the process by which the net

magnetization M_z grows back to its equilibrium value M_0. The rate of change in M_z is proportional to the difference in equilibrium value and current value

$$\frac{dMz}{dt} = \frac{1}{T1}(M_0 - M_z), \tag{2.8}$$

with T1 describing the longitudinal relaxation. Solving equation (2.8) gives

$$M_z(t) = M_z(0)\exp(-t/T1) + M_0(1 - \exp(-t/T1)). \tag{2.9}$$

T1 is the time required for M_z to reach $(1 - 1/e)$ of M_0.

T2 relaxation or transverse relaxation is the loss of transverse magnetization M_{xy}, as originally described by Felix Bloch in 1946. T2 relaxation is considered to follow first order kinetics, resulting in a simple exponential decay (like a radio-isotope) with transverse relaxation rate R2, and its inverse is the relaxation time T2 [8] - sometimes referred to as spin-spin relaxation. *Spin echo* and how to measure T2 is explained further in section 2.2.2. It can also be noted that anything causing T1 relaxation will also create T2 relaxation, but not vice versa.

In practical MRI there are small inhomogeneities in the static magnetic magnetic field creating destructive interference in the FID. The time constant for the observed decay of the FID is commonly denoted by $T2^*$, it is the sum of both static and dynamic dephasing. All three of the above relaxation rates are used as contrast in MRI. T1 is the longest - about one second in soft tissue, $T2^*$ is always shorter than T2. The relation between relaxation rates and relaxation times are given as

$$R2^* = R2 + R2^{'}, \tag{2.10}$$

$$\frac{1}{T2^*} = \frac{1}{T2} + \frac{1}{T2^{'}}. \tag{2.11}$$

The transverse relaxation rate $R2^*$ and its inverse $T2^*$ is found and calculated by measuring the signal intensity versus time t and fitting the curve by e.g. the method of least squares. The resulting function is described as

$$M_{xy} = M_{0xy}e^{-R2^*\cdot t} = M_{0xy}e^{-t/T2^*}. \tag{2.12}$$

In equation (2.12) M_{xy} simply refers to the magnetization vector sum in the transverse plane xy that precesses around the main magnetic field, and M_{0xy} is the sum of the transverse components of magnetization immediately following the RF pulse at an arbitrary angle, preferably 90° for maximum signal.

2.2.2 Free induction decay and the spin echo

The term spin echo comes from a paper by Erwin Hahn from 1950 [9] and is essentially the application of two consecutive RF pulses. First there is the 90° RF pulse - at the Larmor frequency - that effectively flips the spins into the transverse plane. The spins will dephase due to local field variations denoted by $T2^*$, after some time TE/2 another RF pulse with twice the duration of the first turns the dephased spins through 180°. This effectively refocuses the dephasing spins, an echo is conceived at the time TE where signal is recorded. This process can be done several times over producing several echoes before a new 90° pulse. The time between two 90° RF-pulses is called the repetition time TR.

As noted in section 2.2.1 in a real MR experiment the FID decays fast due to $T2^*$ effects. In a spin echo experiment it is the refocused echo that is recorded, each consecutive echo is smaller and corresponds to lack of coherence due to T2 relaxation. A simple way to calculate the constant relaxation rate T2 is to measure the signal intensity for several consecutive spin echoes in a region of interest (ROI) over a range of TEs and then fitting the signal to:

$$S(TE) = S_0 e^{-R2 \cdot TE}, \tag{2.13}$$

according to equation (2.12) where T2 is the reciprocal of R2. In Figure 2.2 the FID and the spin echo following a refocusing (180°) pulse at TE/2 is depicted.

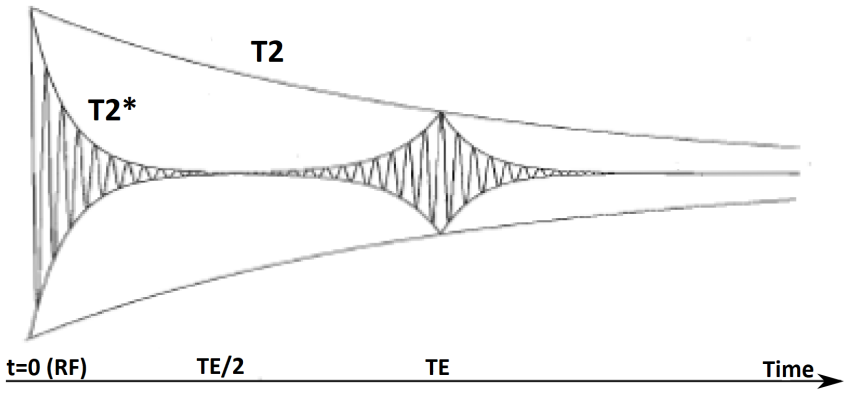

Figure 2.2: The innermost envelope depicts the $T2^*$ decay, at time TE/2 a 180° RF pulse, with equal magnitude but twice the duration as the first is introduced and the resulting echo can be detected at time TE, the outermost envelope signifies the natural or true T2 of the imaged tissue.

In the literature MR sequences are often depicted in a pulse sequence diagram. In Figure 2.3 a single spin echo sequence is presented. Different notations exist, the gradients are called “slice”, “phase” and “read” for the rest of this text. Referring to a slice selective gradient that excites a slice with a chosen thickness through the body or object, the phase encoding gradient is often depicted as a box with many lines referring to different phase encoding lines of *k-space*. The last gradient is called read because it imposes spatial encoding by frequency, and is always turned on when we read out the signal. We measure the signal when it is strongest, at the echo that occurs at time TE as indicated in Figure 2.2, k-space and how the signal is recorded to produce an image is explained in detail in section 2.4.1.

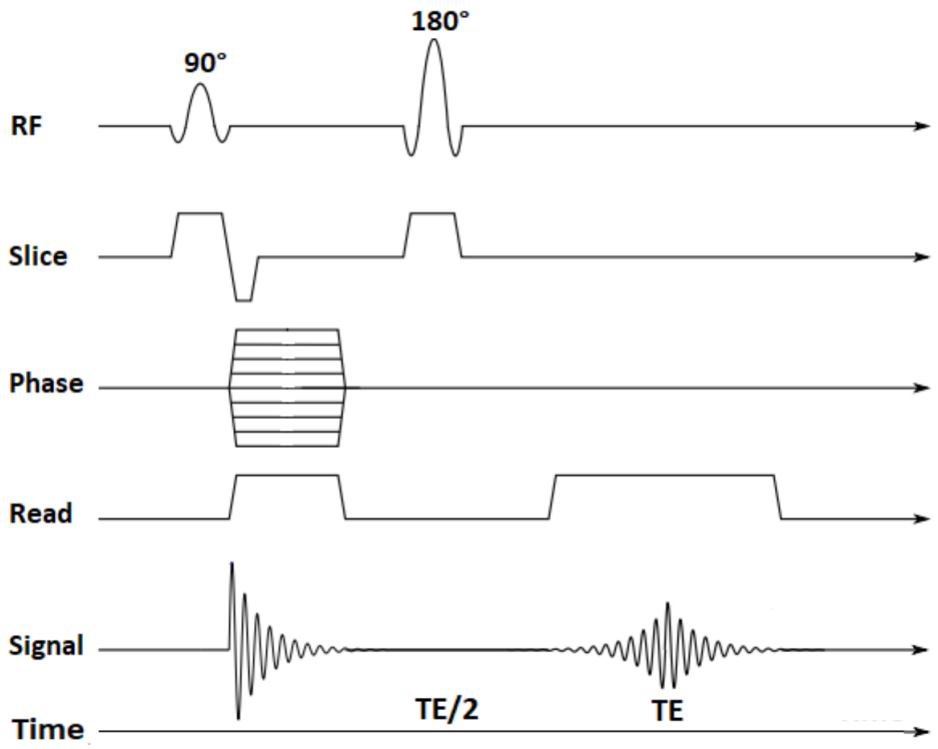

Figure 2.3: A single spin echo sequence. The slice selective gradient is applied simultaneously to the 90° pulse thus exciting a single slice. Then a phase encoding gradient is turned on at the same time as the frequency or read-out gradient. At t = TE/2 a slice selective refocusing 180° pulse is applied and the signal is sampled at the echo occuring at t = TE at the same time as the read gradient is turned on to impose position dependent frequency on the spins in the slice. The sequence is repeated after a repetition time TR.

2.3 Diffusion

Diffusion is the net movement of particles from high chemical potential to lower. A distinguishing part of diffusion is that it depends on the random walk motion of particles and results in mixing without bulk motion. Such movement is called Brownian motion named after Robert Brown in which microscopic particles performs a random walk, Brown discovered the random walk of pollen grains in water in 1827.

2.3.1 Free diffusion

The free diffusion motion can be explained by a one-dimensional random walk from $x = 0$, using the probability distribution of a single particle as explained by [10].

$$P(x,t) = \sqrt{4\pi D t}\, e^{x^2/4Dt}, \tag{2.14}$$

where D is the diffusion coefficient and t is time. The diffusion coefficient D describes the degree of mobility for the particles and $P(x,t)$ is symmetric with expectation value zero. The second moment reduces to

$$\langle x^2(t)\rangle = \int^{\infty} x^2 P(x,t)\,dx = 2Dt. \tag{2.15}$$

Variance is proportional with time so the probability of finding a particle far away from origin increases with time, t. By expanding the dimension $n = 1$ to arbitrary dimension n and assuming a concentration of particles

$$C(\mathbf{r},t) = \int_{-\infty}^{\infty} d\mathbf{r'} C_0(\mathbf{r'}) P(\mathbf{r}-\mathbf{r'},t), \tag{2.16}$$

given that the initial concentration is $C_0(\mathbf{r})$. Applying Fick's law to define the current $\mathbf{j}$

$$\mathbf{j} = -D\nabla C(\mathbf{r},t), \tag{2.17}$$

and inserting the expression for the current $\mathbf{j}$ into the equation of continuity [11]

$$\frac{\partial C}{\partial t} + \nabla\cdot\mathbf{j} = 0, \tag{2.18}$$

the classical diffusion equation is reached:

$$\frac{\partial C}{\partial t} = D\nabla^2 C. \tag{2.19}$$

Equation (2.15) is the specific case for $n = 1$ and $\mathbf{r}_0 = 0$, in general the mean square displacement for a particle after time, t can be written as

$$\langle(\mathbf{r}-\mathbf{r}_0)^2\rangle = \langle\mathbf{r}^2\rangle + \mathbf{r}_0^2 - 2\mathbf{r}_0\langle\mathbf{r}\rangle = 2nDt, \tag{2.20}$$

where $\mathbf{r}$ is the n-dimensional position vector and $\mathbf{r_0}$ is the initial position. Free diffusion is independent of dimension n, in three dimensions the probability surface represents a sphere and the expected diffusion length of a single particle movement after time t is $\sqrt{6Dt}$.

2.3.2 Non-free diffusion

In tissue diffusion is not free due to the presence of cell membranes, fibers and other hindrance. We can in general differ between two types of non-free diffusion. There is *restricted* diffusion - when a particle is trapped inside an object. And there is *hindered* diffusion - when the diffusive particles are in an environment with obstacles. Obstacles hinder the path for diffusing particles, see Figure 2.4.

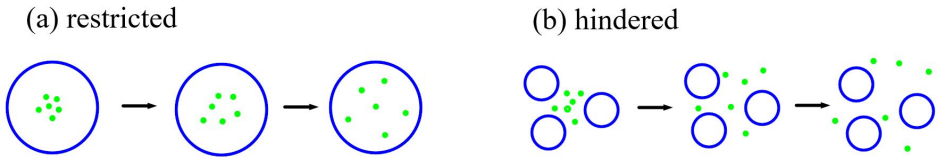

Figure 2.4: Illustration of (a) restricted diffusion and (b) hindered diffusion evolving with time.

If the random walk-motion of particles in the two environments are compared to free diffusion it is clear that the mean squared displacement is less for restricted and hindered diffusion compared to free. For restricted diffusion the mean squared displacement converges to an upper bound relating to the microstructure and can no longer be described by a Gaussian distribution. It is common to refer to the observed diffusion coefficient as the *apparent diffusion coefficient* or ADC - to indicate that the diffusion coefficient is strongly dependent on the interactions of the diffusive particles with the microstructure of the tissue. When introducing a diffusion time Δ the ADC becomes time dependent, see Figure 2.5.

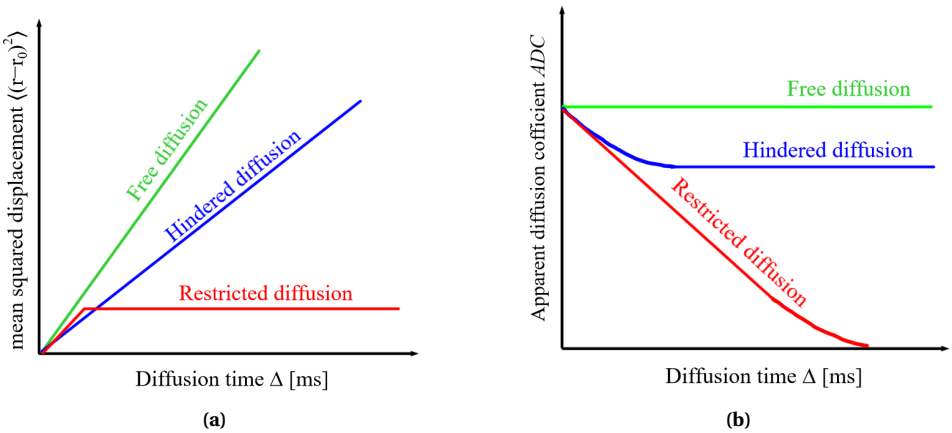

Figure 2.5: (a) The mean squared displacement of diffusing particles in different environments. Free diffusion (green), hindered diffusion (blue) and restricted diffusion (red) as function of diffusion time Δ. (b) Typical behaviour of the ADC in different environments with respect to Δ.

2.4 Image acquisition and pulse sequences

2.4.1 K-space and the Fourier Transform

The coverage of k-space is pivotal to reconstructing an image of the sample by the inverse Fourier Transform. Imaging of a body in MR is in essence measuring the proton density from the signal generated by precessing spins, a signal containing both frequency and phase information [2]. The physical signal that is measured in the receiver coils are effectively a Fourier Transform of the spin density. In this section the key concepts of k-space and how it is used to produce an image will be addressed.

First of all it is necessary to consider relaxation effects, data sampling must be done when the signal is large enough to give sensible information, either close to the initial RF, in the FID or at an echo. Given only the static field B_0 the frequency of precession ω_0 is the same throughout the body. A gradient field has to be added for spatial localization, when a gradient field G is present the frequency ω is a function of position determined by the strength of G. Phase information is a function of both position and time. The demodulated MR signal $S(t)$ generated by precessing nuclear spins in the presence of G is the Fourier Transform of the effective spin density, ρ_{eff}

$$S(t) = \rho_{\text{eff}}\big(\vec{k(t)}\big) \equiv \int_{-\infty}^{\infty} d\vec{x}\rho(\vec{x}) \cdot \exp(2\pi i \vec{k}(t) \cdot \vec{x}), \tag{2.21}$$

introduced by Ljunggren[12] and Twieg [13] independently in 1983, where

$$\vec{k}(t) \equiv \int_0^t G(\tau)d\tau. \tag{2.22}$$

As time progresses the signal traverses through k-space with the velocity vector of the trajectory proportional to the field gradient, G. $\vec{x}$ is the sampled data in k-space as defined by the phase and read-gradient, see Figure 2.3. By effective spin density, we mean the true spin density $\rho(\vec{x})$ corrected for the effects of T1 preparation, T2-decay and dephasing from T2*, flow effects or diffusion.
To reconstruct an image $I(\vec{x})$ the inverse Fourier Transform of the sampled data is computed,

$$I(\vec{x}) = \int_{-\infty}^{\infty} d\vec{k} S\big(\vec{k}(t)\big) \cdot \exp(-2\pi \vec{k}(t) \cdot \vec{x}) \tag{2.23}$$

Each individual pixel in k-space does not correspond one-to-one to a pixel in the actual image. Each point in k-space contains spatial frequency and phase information about every pixel in the final image. Conversely, each pixel in the image maps to every point in k-space. The two directions of k-space are the phase encoding direction and read or frequency encoding direction. Which one is vertical or horizontal is chosen based on the geometry of whatever is in the scanner. In Figure 2.6 there is a representation of an actual image and its Fourier Transform or k-space equivalent.

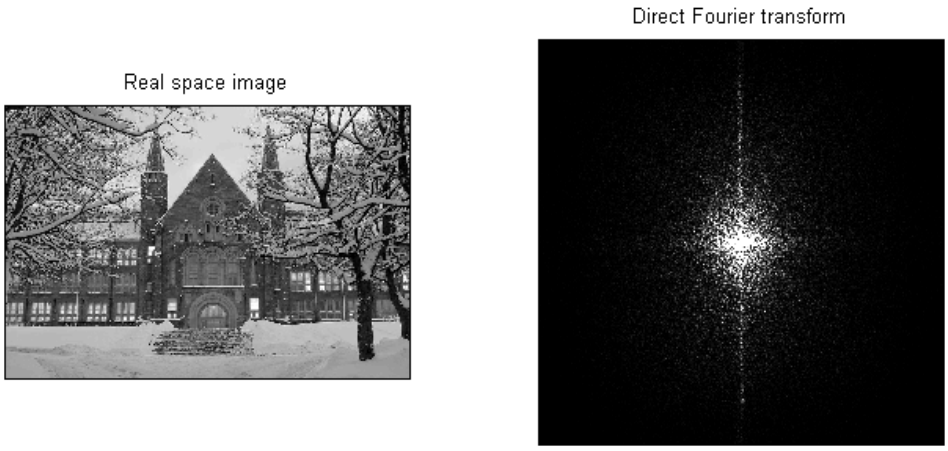

Figure 2.6: Representation of how the Fourier Transform of a real image looks like, no information is lost in the process and both images can be created from the other. In MRI we record k-space and reconstruct the image of the body by the inverse Fourier Transform. Image produced using MATLAB.

K-space in MRI looks roughly equal to the right image in Figure 2.6 and has the same

type of symmetry. However in MRI we acquire the k-space image first and reproduce the real image afterwards. One can imagine a picture as being composed of waves with different amplitudes and frequencies, the Fourier Transform separates combined sine waves into their individual components. In the centre of k-space lies the lowest frequencies of the image, this corresponds to basic image contrast, e.g the blackness of the trees compared to the white in the snow, in Figure 2.6. Radially outward at the edges of k-space are the highest amplitudes and frequencies, they correspond to borders and edges in the image, e.g the branches and outlines of different objects in the image. There is also conjugate symmetry for real objects in k-space that allow for the time saving technique of partial Fourier reconstruction. A fraction of k-space can be constructed from symmetry to save time while scanning.

2.4.2 Echo planar imaging

Echo planar imaging or EPI is in general a broad term covering a number of different sequences. The key element of EPI is that all or most of k-space is filled up following a single RF excitation, then the sequence is popularily named a single-shot EPI. Although there exists multishot EPI where a small number of excitations is used to image an entire slice. In the FID or in a conventional spin echo a *gradient echo* or GRE can be made by applying an alternating gradient. By doing so the dephasing is accelerated, but it can be reversed by a rephasing gradient that has the same strength but opposite polarity. T2 and T2* processes are unaffected by the gradients and several GREs can be be produced in rapid succession in the span of the FID or within a spin echo. A Spin echo sequence can have an EPI-readout meaning several GREs are made to acquire all the necessary lines of k-space in one go - whithin the conventional spin echo. The advantages of EPI readout is that it is fast and reduces the effects of patient movement. Mansfield described the process in 1977[14] and his group produced the first EPI images in the early 1980s. In Figure 2.8 is a sequence diagram of a spin echo-EPI, meaning a spin echo protocol with an EPI readout.

The effectiveness of the EPI sequence is apparent from Figure 2.8 due to several or all lines of k-space being recorded within a single TR. Every time the phase encoding gradient is turned on (commonly called a 'blip') a new phase line is recorded by alternating the read gradient after each phase-blip. Another way of saving time in imaging is partial Fourier reconstruction, taking advantage of the conjugate symmetry of k-space as mentioned in section 2.4.1 and record some fraction of k-space with a single-shot EPI and then reconstruct the image from symmetry. When doing partial Fourier it is impor-

tant to include sufficient coverage of the center of k-space so as to not loose contrast. In a single shot EPI the entire k-space is filled in a zig-zag manner, a visualization is provided in Figure 2.7.

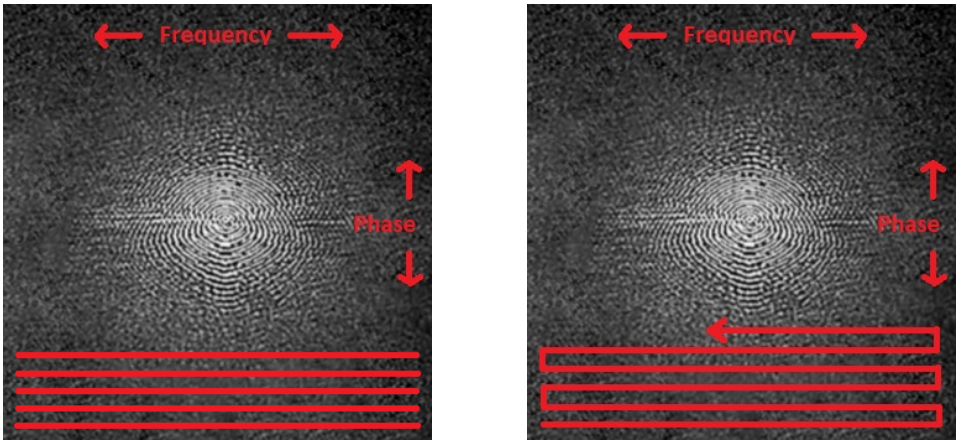

(a) (b)

Figure 2.7: (a) In a spin echo sequence only one line of k-space is filled after the initial 90° RF-pulse, and a new line is recorded at another phase encoding after time TR, see Figure 2.3. (b) The EPI sequence is constructed in such a way that all of k-space can be recorded within one TR. The vertical axis is phase and the horizontal is frequency or read. A simplified schematic of the sequence protocol is presented in Figure 2.8.

It is only the readout of the EPI that separates it from e.g. a conventional spin-echo sequence, everything up until t = TE/2 is exactly similar in a spin echo-EPI compared to a regular spin echo experiment. To compare EPI with conventional spin-echo, it is useful to compare the speed of the imaging sequence. In spin-echo, one line of imaging data in k-space is recorded within each TR. If there is 128 phase encoding steps (or lines of k-space) and TR = 2 seconds then the imaging time is 256 seconds or 4 minutes and 16 seconds. If the signal is averaged over multiple RF excitations the imaging time increases proportionally. In an EPI sequence the frequency or read-gradient oscillates between positive and negative amplitudes creating a train of gradient echoes or lines of k-space. Each line or GRE is phase encoded differently by a phase encoding blip, see Figure 2.8. The total scan time of the EPI sequence depend on the number of excitations needed to fill k-space and the averaging, but is significantly faster compared to spin echo.

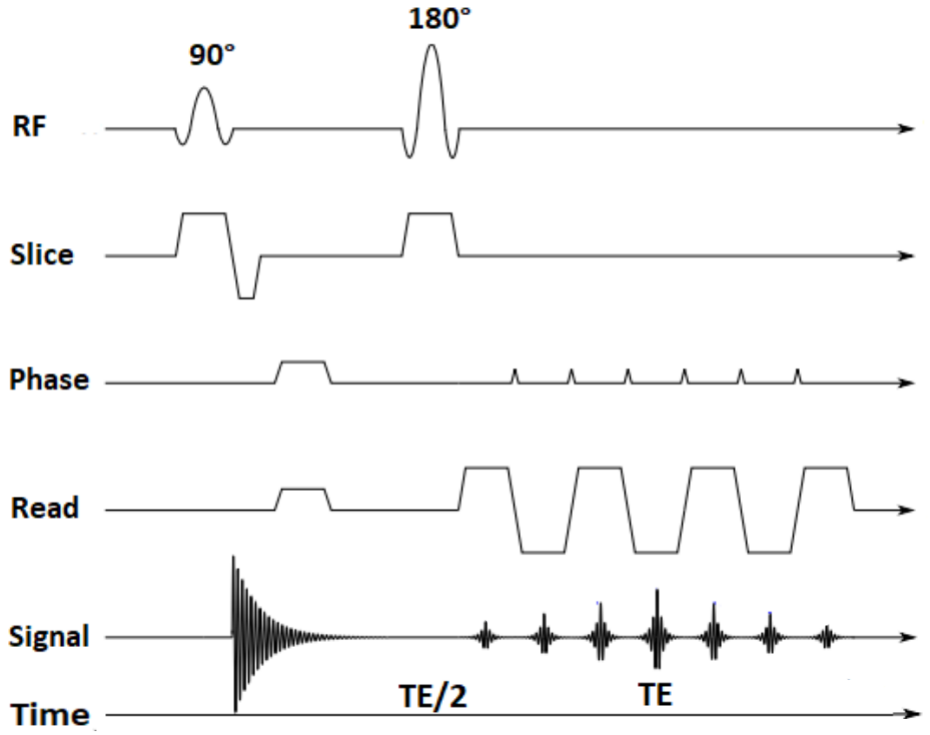

Figure 2.8: A 90° pulse applied with the slice selective gradient excites a single slice. A single phase and read gradient is turned on followed by a slice selective 180° refocusing pulse. The readout gradient changes direction with each phase blip thus recording another line of k-space with each GRE indicated on the signal curve. The centre GRE is at the middle of the regular spin echo and has the largest amplitude. Note that this is a simplified sequence diagram, a real EPI sequence has a lot more GREs to sufficiently cover k-space.

2.4.3 Diffusion weighted imaging

Brownian motion or diffusion, as explained in chapter 2.3 is an important feature of many physical systems, and is a characterizing property of tissue. Mapping the diffusion of e.g. water in biological tissue helps to create a better understanding of the true microstructure. The sensitivity of the spin-echo signal on molecular diffusion was recognized by Hahn in 1950, he reported a reduction of signal and explained it in terms of the dephasing of spins caused by translational diffusion within an inhomogeneous magnetic field[4]. Four years later Carr and Purcell provided a complete mathematical and physical framework for measuring diffusion in biological tissue using Hahn's spin-echo sequence[15]. A spins precessional frequency is determined by the local magnetic field B as stated by the Larmor equation (2.1). If a magnetic field gradient is applied, spins at different positions experience different magnetic fields - thus precessing at different frequencies. After a certain time the spins acquire different phase shifts depending on their location. Stronger gradients lead to larger phase shifts and a higher sensitivity to diffusion. By turning on a gradient G before the 180° pulse a position dependent phase shift is introduced, a second G after the 180° turned on for an equal amount of time as the first, producing a negative phase shift that reverses the first will cause no net phase shift for stationary spins. In clinical MR a value called b is used to quantify the sensitivity of diffusion. The most common sequence for diffusion weighted imaging or DWI is the method proposed by Stejskal and Tanner [16], the diffusion weighting b is proportional to the square of the gradient strength:

$$b = \gamma^2 G^2 \delta^2 (\Delta - \delta/3). \tag{2.24}$$

Where γ refers to the gyromagnetic ratio of protons - same as in the Larmor equation, G is the gradient strength and δ is the gradient duration. Δ is the time delay from the leading edge of the first gradient to the end of the other [17]. When $\delta \ll \Delta$ the expression for b is sometimes simplified as: $b = \gamma^2 G^2 \delta^2 \tau$ where $(\Delta - \delta/3) = \tau$, and τ is the diffusion time - in this thesis the diffusion time is defined as Δ. Protons in water that change location between the two gradient pulses will not be properly phased at the time of readout - resulting in reduced signal. Diffusion sensitizing gradients G can be added to a spin echo-EPI sequence. Since patient movement will completely overwhelm the molecular diffusion that we try to measure, a fast imaging technique is required, such as spin echo-EPI, depicted in Figure 2.8. In the time between the two gradients, displacement occurs in diffusive tissue, resulting in a lower signal because out of-phase

spins will cancel each other out. Resulting signal is given by

$$S(b) = S_0 e^{-bD}, \tag{2.25}$$

S_0 is the signal intensity with no diffusion weighting, b is the b-value and D is the diffusion coefficient. It is important to note that diffusion in biological tissue is not in general isotropic, but dependent on the microstructure of the tissue. When performing DWI we cannot measure the true diffusion coefficient D instead we estimate the apparent diffusion coefficient ADC, an estimate of the mean diffusion in each voxel. In general, to determine ADC one needs to acquire images at multiple b-values or at least one b-value > 0 apart from $b = 0$ s/mm^2 and then fitting the signal to equation (2.25). The simplest approach for acquiring ADC without fitting is by using only two b-values then the closed form solution is the following:

$$ADC = \frac{1}{b_2 - b_1} ln(\frac{S(b_1)}{S(b_2)}, \tag{2.26}$$

where $b_1 < b_2$, $S(b_1)$ and $S(b_2)$ are the signal intensities at $b = b_1$ and b_2, respectively [17]. For obvious reasons a better method is that of several b-values and exponential fitting according to equation (2.25) thus giving an estimate for the ADC but not necessarily equal to the true diffusion coefficient D. The estimation of ADC will most likely be affected by the diffusion time Δ, see Figure 2.5 and whether or not to include $b = 0$ s/mm^2 in the calculation will also affect the final result.

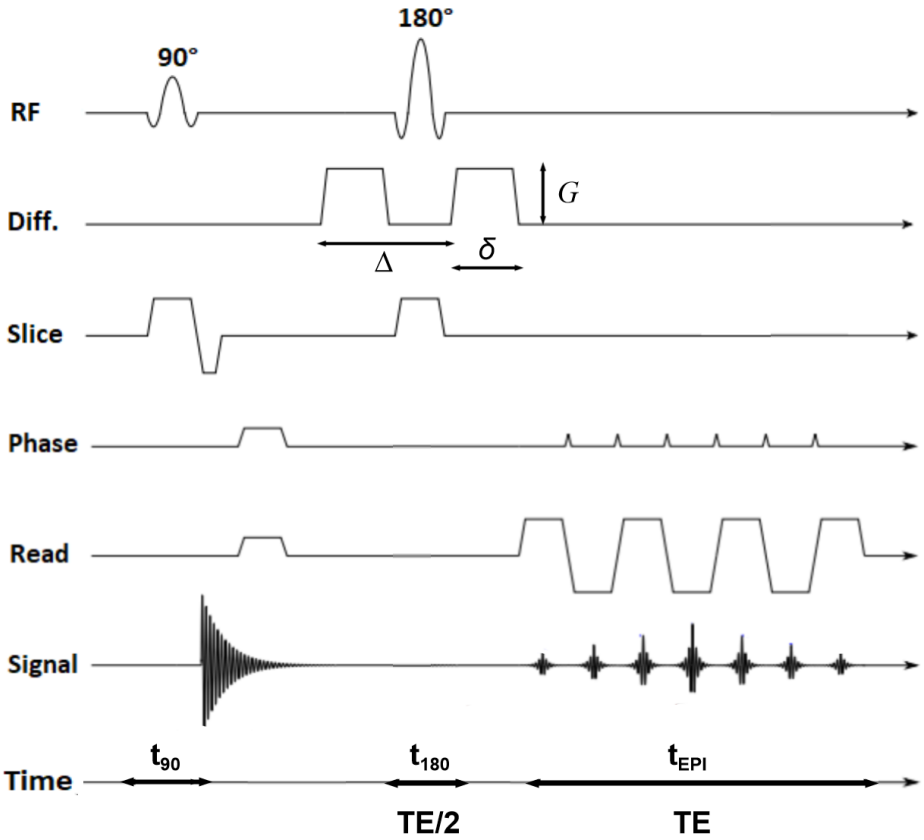

Figure 2.9: A typical diffusion weighted EPI sequence with additional diffusion sensitizing gradient (Diff.). The 90° pulse is slice selective, phase and frequency encoding is similar to an EPI sequence in this diagram, before the 180° pulse a diffusion gradient is turned on followed by the 180° pulse and another diffusion gradient reverting the phase difference from the first gradient to stationary spins. Readout is similar to a regular EPI sequence with no diffusion weighting as shown in Figure 2.8. This particular protocol is more commonly known as a Stejskal Tanner-sequence [18] with monopolar gradients and an EPI readout. The duration of one diffusion gradient is δ and the time from the leading edge of the first gradient to the second is the diffusion time Δ. G is the strength of the diffusion gradient and is limited by the performance of the scanner.

2.5 Noise vs background

Noise effects in diffusion MRI data underscores the need for post processing and fitting of the image signal over a range of b-values to a model. However, fitting algorithms are sensitive to the noise structure and measurement errors. In magnitude reconstructed images one particular source of systematic error occurs due to the non-Gaussian nature of the noise, prominent at high b-values - resulting in a systematic shift from a noise-free signal [19]. Two subgroups of noise are addressed, intrinsic background and variance in the measured signal.

2.5.1 Signal to noise

The signal to noise ratio (SNR) is frequently measured in MRI by calculating the difference in signal intensity between an area of interest and the air. The difference is then divided by the standard deviation of the background signal which indicates the variability of the noise in the air. A lower SNR generally results in a grainy appearance in an image. SNR is affected by the type of sequence, it can be improved by tweaking the scan parameters, e.g averaging, increasing FOV or decreasing matrix size [20–22]. Signal noise in MRI is often modelled after a Rician distribution model as derived by Rice [23].

2.5.2 Rician distribution

The noise in the MR signal can be described as an additive complex contribution to the pure MR signal. In general if the real and imaginary part of a phase modulated signal is corrupted by Gaussian noise with a normal distribution $n(\mu,\sigma)$ then the statistics R of the signal will follow a Rician distribution. Mathematically this signal can be described as

$$R = R_{\mathrm{Re}} + iR_{\mathrm{Im}}, \tag{2.27}$$

where R_{Re} and R_{Im} is the real and complex noise contributions in the image domain respectively [24]. The real and imaginary parts of the noise are still zero mean with σ^2 variance Gaussian signals.

Noise variables are assumed to be Gaussian as long as there is no bias in the system setup. Common practice in MRI is to work with magnitude images rather than complex ones. When recording a signal the absolute magnitude noise $|m|$ is given as:

$$|m| = \sqrt{R_{\mathrm{Re}}^2 + R_{\mathrm{Im}}^2}. \tag{2.28}$$

The measured signal S_m with standard deviation σ is affected by the magnitude noise $|m|$ and the source of error is particularly prominent when SNR becomes low, either with long TE or at high b-values. The main effect of such noise is that the signal reaches a noise floor and does not reach zero. The nominal value μ of the true signal S is shown for clarity in Figure 2.10 and the offset from zero is κ.

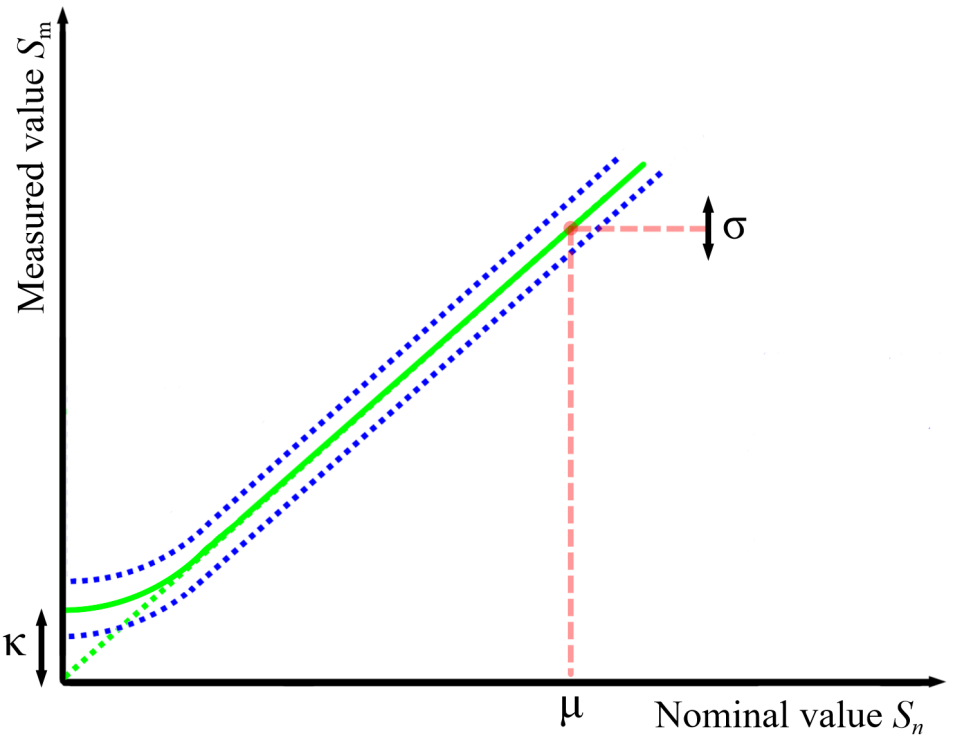

Figure 2.10: Measured and true signal is related to κ as $S_m^2 = S^2 + \kappa$, noise correction of DW-MRI signal is based on an experimental retrieval of κ with a Phantom scan. The solid green line is the measured signal S_m and the dashed green line is how signal would behave without any noise and reaching zero. Blue dashed line indicate the variance in the measured signal.

For noise correction in a DW-MRI sequence an experimentally obtained noise correction factor NCF is obtained relating to the offset κ due to the magnitude noise $|m|$.

2.5.3 Noise correction factor NCF

Diffusion MRI data from a DWI protocol is prone to noise and requires some signal processing to a model. The signal to noise ratio is lower for higher b-values, the most prominent effect of noise on the signal is attenuation at high b-values when SNR is low

and signal reaches a noise floor. Simple monoexponential fitting of signal can cause underestimation of ADC. Unfortunately it is not trivial to retrieve true signal from noise corrupted data. In biological tissue a region of interest can be quite inhomogenous and the standard deviation of the signal intensity can be quite large even with an averaging approach. Even the background noise surrounding the object can be quite inhomogenous and the positioning of a pure noise ROI is not straigh-forward, the actual noise figure might not have a analytical solution [25].

In this section a method for estimating noise based on the work by Le Bihan et al. [26] is presented. A Noise correction factor, NCF is obtained experimentally through a DWI protocol. The correct signal intensity S is related to the measured signal S_{m} as:

$$S_{\mathrm{m}}^2 = S^2 + \mathrm{NCF} \tag{2.29}$$

The parameter NCF characterizes the intrinsic noise contribution from the acquisition setup and from images made in a free diffusion phantom with known diffusion coefficient D. The signal decay follows a monoexponential equation $S = S_0 \exp(-bD)$, where S_0 is the signal at $b = 0$. Thus equation 2.29 can be written as

$$S_{\mathrm{m}}(b)^2 = S_0^2 \exp(-2bD) + \mathrm{NCF}. \tag{2.30}$$

The NCF is a measure of the deviation of S_{m}^2 from the monoexponential law. Once NCF is determined from the phantom images the noise corrected signal can be obtained from any type of structure provided the acquisition sequence and set-up remains the same. A simple SNR expression can also be found using the NCF.

2.6 The female breast

The female breast is composed of adipose tissue (fat), glandular tissue which makes and transports milk, connective tissue for support, blood for nourishing the tissue and lymph nodes for waste removal, water is a key element in most of the above inside the cell as well as outside, except for in fat, or at least to a very small degree. The structure within the breast is not trivial and a small region can contain several different types of tissue. In Figure 2.11 is a schematic of a healthy female breast.

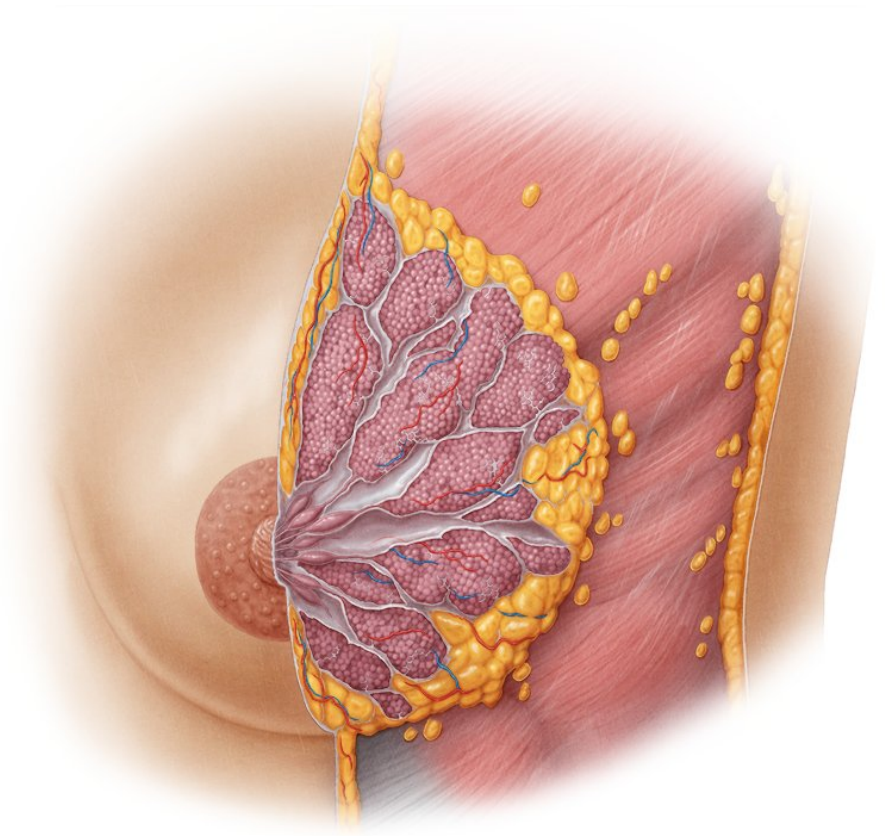

Figure 2.11: A cross section schematic of mammary glands, underneath the breast are the pectoralis muscles and inside the breast adipose tissue is shown as yellow, the fibroglandular tissue is shown in pink lobes with the milk ducts leading up to the areola.

Breast tissue in a broad manner means two major tissue types: Fibroglandular tissue (FGT) and adipose tissue (fat). In an MRI of breasts it is important to suppress as much as possible of the fat signal to get a good image of FGT. Three commonly used techniques for fat suppression is inversion recovery, fat-saturation and opposed phase imaging [27]. In Figure 2.12 a biopsy sample of healthy breast tissue is shown. The sample is stained with Hematoxylin-eosin-saffron, abbreviated HES. HE is one of the primarily used stains in histology, HES is preferred in FGT and other collagen rich environments due to saffron coloring the collagen fibres yellow. Cell nuclei are blue or purple while muscle and elastic fibres are pink.

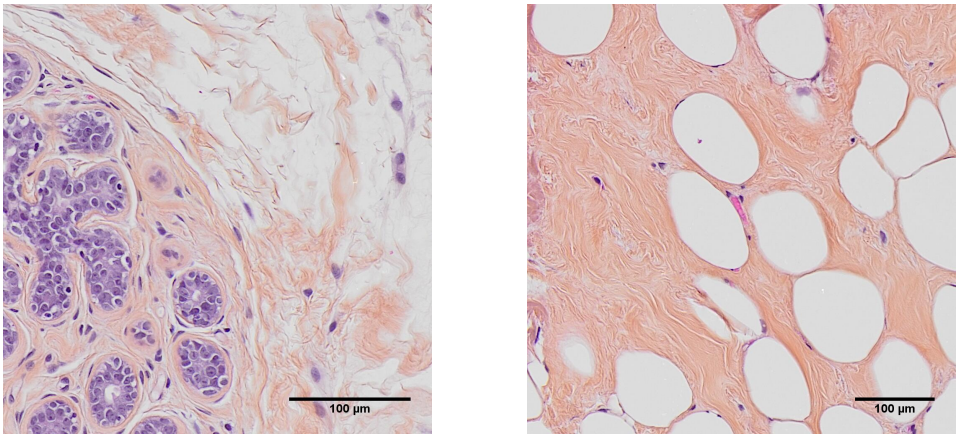

(a) (b)

Figure 2.12: (a) A HES stained biopsy sample of healthy breast tissue, in yellow is connective tissue (collagen) in a swirly healthy pattern, the purple cells (erythrocytes) surround milk ducts and represents the glandular tissue. White voids might be drying cracks from sample preparation. The purple cell clusters are milk ducts. (b) Another sample showing the collagen and white adipose tissue in large circular clusters.

2.6.1 Tortuosity

In diagnostic oncology of breast tissue there are several potential biomarkers for malignant cancers. There is the change in tissue composition and pathology that can be highlighted in a T2 weighted image due to change in transverse relaxation or an elevated signal in DWI due to reduced ADC in the tumor microenvironment [28]. It is in general accepted that reduced ADC in tumor tissue is due to high packing density of cancer cells in these lesions - however the physical mechanism remains unclear [1]. One possible explanation for the lowered ADC values due to greater cell packaging is the decrease of

extracellular space volume fraction and increased tortuosity of the extracellular space matrix. The tortuosity of an environment describes the shortest possible trajectory S^* compared to the true distance S between two arbitrary points, as the fraction:

$$\alpha_S = \frac{S}{S^*}. \tag{2.31}$$

A geometrical image of tortuosity would be if one imagines running through the woods, increased tortuosity means more hindrance and more trees to run around. An unhindered path means α_S reaches unity. Another common picture of tortuosity is the meandering river, in breast tissue a physical measure is the fraction of the ADC over the true diffusion coefficient D, alternatively for long diffusion times

$$\alpha_D = \frac{ADC}{D}. \tag{2.32}$$

Decreased extracellular space typically leads to more hindrance for extracellular water molecules, and increased tortuosity. Less mobility for water molecules in the extracellular space means decrease in ADC - as is common for lesions.

2.7 Two potential Biophysical models of breast tissue

2.7.1 Two compartment model

Assuming that the MR signal originates from water protons there are only two regions for the water to exist in. One compartment is within the cell, intracellular water. The other compartment is the extracellular water - outside of the cell. Due to the restricted environment of the intracellular water and the tortuous, hindered environment of the extracellular, each compartment is expected to have its own unique ADC- and T2-values. In the intracellular compartment water molecules are restricted within the cells themselves. Restricted diffusion of intracellular water has been detected and theoretically modelled in many biological systems [29]. If the fraction of extracellular to intracellular water is f then the signal S can be modeled as:

$$S = S_0(fe^{-TE/T2_1}e^{-b\cdot ADC_1} + (1-f)e^{-TE/T2_2}e^{-b\cdot ADC_2}), \tag{2.33}$$

where subindex 1 refers to the largest compartment, extracellular and 2 for intracellular and S_0 is the signal with no diffusion weighting, $b = 0$. The resulting signal from a DWI sequence is then considered to behave as a bi-exponential function dependent on the characteristic T2 and ADC for each compartment.

2.7.2 Alternative model

An alternative model is based on the assumption that the ADC is related to diffusion time Δ as ADC(Δ). The signal S is then modeled as

$$S = S_0 e^{-b \cdot ADC(\Delta)} e^{-TE/T2}, \tag{2.34}$$

where S_0 is the signal for $b = 0$ s/mm^2 and Δ is the TE-dependent diffusion time, see Figure 2.9. If the signal attenuation at non-zero diffusion weighting is dependent on the duration of Δ then the observed signal behaviour could be a result of prolonged diffusion time at longer TE. T2 is important because it provides insight in the expected quality of the diffusion weighted images, a decrease in T2 exponentially decreases the attenuation of DW signal. But how does echo time and the duration of Δ affect the ADC? On one hand, an increase in TE and consequently Δ decreases SNR for the overall signal due to T2 relaxation. Simultaneously the change in the measured ADC could occur due to the different behaviour of diffusive particles in their respective environment, hindered and restricted. The alternative model is a single compartment model and the mean squared displacement of diffusive particles is a function of diffusion time Δ given strictly by the duration of TE as programmed by the scanners protocol. T2 is assumed constant in the alternative model.

2.8 Optimization of protocol

The optimization is conditioned by a lower and upper limit of the b-value and a fixed number of acquisitions. The assumption in the presented optimization framework is that the signal is adequately described by equation (2.25) for the diffusion weighted signal at both lower and upper bound.
Changing the echo time TE also means changing the duration of the diffusion gradient, δ. The gradient strength G also changes depending on the b-value, but is restricted based on the available gradient strength. The echo time in the DW-MRI sequence is defined as:

$$TE = 2 \cdot \delta(G, b) + t_{90} + t_{180} + t_{\text{EPI}}. \tag{2.35}$$

In a diffusion weighted spin echo-EPI the $\delta(G, b)$ is the duration of the diffusion encoding gradient in real time, t_{90} and t_{180} is the duration of the 90° pulse and 180° pulse respectively, t_{EPI} is the time for the readout, see Figure 2.9. Due to the restrictions imposed by the maximum available gradient strength G a limitation on b for a given TE and vice versa can be estimated analytically from equation (2.24).

For optimization of imaging protocol it is important to measure T2 since it affects the quality of the diffusion image to a large extent. The combination of T2 and TE exponentially decreases the DW signal, combined with b and ADC the signal S is described by the relation:

$$S = S_0 \exp(-TE/T2)\exp(-b \cdot ADC), \tag{2.36}$$

where S_0 is the signal for $b = 0$ s/mm^2. Measuring T2 and ADC separately gives a prediction of what SNR one might expect in a DW image according to the above relation. Knowing both T2 and ADC serves as a simple guide for choosing a range of TE and b with a desired SNR according to equation (2.36).

Chapter 3

Methods

All collected MR data was recorded on a MAGNETOM - Skyra, 3 T scanner (Siemens healthcare, Erlangen, Germany) [30]. Specifications of the system is given in Table 3.1.

Table 3.1: Specifications of the Siemens MAGNETOM - Skyra, 3 T-scanner.

Field Strength	3 T
Bore size	70 cm
Magnet length	163 cm
System length	173 cm
Gradient strength	45 mT/m
Slew rate	200 T/m/s
Shimming	passive and active

Three healthy female volunteers were included in this study and provided written informed consent to undergo a series of MRI examinations including DW-MRI.

3.1 Observations

A specialization project in physics was carried out by the author of this thesis in the fall of 2018 with the title "T2 mapping in breast tissue, phantom and fruit: comparison of four different pulse sequences". Monoexponential fitting of transverse relaxation was done in order to estimate T2 in a variety of phantoms and in the healthy breast tissue of three female volunteers. An interesting observation from that project was that the assumed constant T2 value in fibroglandular breast tissue increased with diffusion weighting b. Thus, there is a signal contribution in the diffusion weighted signal for high

b-values that contributes to the transverse relaxation. Mapping of T2 is done again in this research and the same observations persists. This thesis aims to find a biophysical model of breast tissue that explains this behaviour in terms of T2 and the apparent diffusion coefficient ADC - an extension of previous research.

3.2 Phantom scan for noise correction, February 2. 2019.

In a diffusion weighted MRI sequence the signal is attenuated due to non Gaussian diffusion according to 2.5.2. To estimate the amount of intrinsic noise in the DWI sequence the same protocol that was used for the healthy volunteers was done on a phantom with known diffusion coefficient D. To accurately estimate the intrinsic noise in the protocol an additional scan where the b-value range was stretched to 3600 s/mm^2 with a corresponding echo time, TE = 170 ms, was made. It is fair to assume that the scan with long TE and high b-values are primarily noise. The semilog-plot of signal versus b-value will deviate from a descending line and flatten when the noise is dominating the signal, thus allowing for experimental retrieval of NCF. With a known correction factor from a phantom DWI experiment, any DW-MRI data acquired from patients with the same protocol can be corrected for with equation (2.29).

3.3 Direct mapping of biomarkers T2 and ADC

Choosing ROIs were done by the author without prior experience in this kind of work and several attempts were made and analyzed to investigate the effect of poor or good fat suppression, phase direction bias, image artfifacts such as Eddy currents or chemical shift were accounted for.

3.3.1 Protocol parameters

Table 3.2: Protocol parameters for DW-MRI scans. A different number of averages was applied depending on the b-value, one for $b = 0$, 3 for $b = 100$ and 6 for $b = 700$ s/mm^2.

TE [ms]	TR [ms]	b [s/mm^2]	δ [ms]	Δ [ms]
56	5800	0 100 700	11.2	24.9
76	5800	0 100 700	21.2	34.9
96	5800	0 100 700	31.2	44.9
116	5800	0 100 700	41.2	54.9

Table 3.3: Specifics of breast DW-MRI scans.

Fat suppressions	On
Diff. directions	3
Diff. scheme	Monopolar (Stejskal-Tanner)
PAT factor	2
Bandwidth (Hz/Px)	1786
Echo spacing (ms)	0.62
Slice thickness (mm)	3
voxel size (xyz mm)	$2.5 \times 2.5 \times 3.0$
FoV read (mm)	350
FoV phase (%)	98.6
Phase partial Fourier	6/8

3.3.2 T2-mapping

A non-linear least squares method was performed in MATLAB [31] to estimate T2 as described by equation (2.13). ROIs in fibroglandular breast tissue was made with Radi-Ant DICOM viewer 4.6.9 [32]. The echo times in the DWI protocol are listed in Table 3.2 along with δ and Δ in addition to b for ADC-mapping at each TE.

3.3.3 ADC-mapping

The same sequence is used to compute both T2 and ADC. Analogous to estimation of T2 the ADC-values in FGT for all healthy volunteers was computed in MATLAB with a non linear least squares method fitted to equation (2.25). In addition a closed form solution for ADC exists for using two b-values, the analytical solution is computed according to equation (2.26) that is excluding $b = 0$ and only calculating ADC with $b > 0$.

3.4 Biophysical models

3.4.1 Fixed parameters

The lack of available experimental data makes it difficult to precisely model the intrinsic diffusion constants and relaxation rates [1]. Assuming that water in the FGT is divided into intracellular and extracellular water the numerical value of the fraction in the two compartments is based on the literature. Springer et al., 2014 measured the extracellular volume fraction of water in breast tissue and reports a fraction $f = 0.73$ for the extracellular water in FGT as a mean value for a cohort of 11 patients [33]. Sahin and Aribal, 2013 reports a mean ADC in healthy FGT to be $1.42 \pm 0.17 \times 10^{-3}$ mm^2/s whilst

benign lesions show a higher ADC of $1.9 \pm 0.45 \times 10^{-3}$ mm^2/s and malignant lesions have significantly lower ADC of $0.86 \pm 0.26 \times 10^{-3}$ mm^2/s [34]. Assuming the extracellular compartment is largest in healthy tissue that compartment contributes most to the signal. The difference in ADC between malign and benign lesions is most likely due to change in packing density of cancer cells in these lesions. $T2_1$ is set to be closely related to the T2 value of breast tissue found in the literature [35] and closely relates to the measured value found by the author, $T2_1 = 60$ ms. Even though Sahin and Aribal reports an ADC in healthy FGT to be $1.42 \pm 0.17 \times 10^{-3}$ mm^2/s this is significantly lower than the experimentally measured value for a single compartment model and evaluated on the group of healthy volunteers. ADC_1 is set at 1.82×10^{-3} mm^2/s which is the mean ADC measured in an ROI of FGT in the right breast of three healthy volunteers - assuming a single compartment model. ADC_2 is set at 0.2×10^{-3} mm^2/s which is close to 10% of the extracellular ADC commonly used in the literature [1]. The current understanding is that DWI actually measures the signal from the extracellular diffusion of water molecules. The speed of the diffusion is influenced by the ratio of the volume occupied by the cells to the volume of the extracellular space, the composition of the extracellular space (tortuosity) and temperature [36]. The free parameter that is estimated based on the two compartment model is the $T2_2$, the transverse relaxation time of restricted water molecules in the smallest, intracellular compartment. A summary of the constants used in the two compartment model is found in Table 3.4.

Table 3.4: By reducing the degrees of freedom in the two compartment model to only the transverse relaxation $T2_2$ of the intracellular compartment a best possible fit to experimental data is computed based on the assumptions of the model.

$T2_1$ [ms]	$T2_2$ [ms]	ADC_1 [mm^2/s]	ADC_2 [mm^2/s]
60	free variable	1.82×10^{-3}	0.2×10^{-3}

3.4.2 Two compartment model

A computed numerical value for the intracellular T2 is heavily influenced by the fixed parameters in section 3.4.1. To find a best possible fit of model behaviour to experimental data a semi-log plot of signal versus echo time TE is used for easier comparison of measured signal attenuation to bi-exponential model. The main goal is to find a best possible fit for high b-values, in particular for $b = 700$ s/mm^2 as according to experiment.

3.4.3 Alternative model

In the alternative model the assumption is that the computed ADC in a three b-value scheme for each TE varies as a function of increased diffusion time Δ. Δ increases by 10 ms from 24.9 ms at TE= 56 ms for every 20 ms of increased TE according to Table 3.2. This is simply due to how the sequence is programmed. 20 ms of added TE is divided equally in both δs, see Figure 2.9.

Using the recorded signal for non-diffusion weighted images as S_0, the diffusion weighted signal S when $b \neq 0$ s/mm^2 is modeled according to the ADC at each Δ given by TE according to $S = S_0 \exp(-b \cdot ADC(\Delta))$ and compared to experimental values. The ADC(Δ)-values used is the average ADC generated from a mono-exponential fitting according to equation (2.25) for all healthy volunteers.

3.5 Optimization of protocol

The lowest non-zero b-value used in this study was $b = 100$ s/mm^2, the highest b-value was $b = 700$ s/mm^2. The highest b-value should be low enough to ensure that the diffusion weighting is well approximated by a mono exponential model (2.25). The lower and upper limit of b are typical threshold values found in the literature [37]. The range of echo times are listed in Table 3.2 and the maximum available gradient strength G is 45 mT/m at 200 T/m/s. Given such rapid rise time for the gradient - less than 0.2 ms to reach maximum, the strength of G is assumed constant for the entire diffusion gradient and the maximum available b-value, $b_{\max}$ is calculated according to $b = \gamma^2 G^2 \delta^2 (\Delta - \delta/3)$ with the parameters δ and Δ listed in Table 3.2.

The signal attenuation in DWI due to T2 relaxation is in theory a simple relation between the combination of the intrinsic T2 value of the tissue in question and the length of TE. Regardless of b-value the signal S is attenuated by $\exp(-TE/T2)$. Attenuation of signal as a function of b and ADC is also in theory simple ($\exp(-b \cdot ADC)$) however both T2 and ADC is observed to vary depending on parameters TE and b which makes their combined contribution to the DW signal non-trivial. The measured signal in DW images is described by the relation:

$$S = S_0 \exp(-\frac{TE}{T2}) \exp(-b \cdot ADC), \tag{3.1}$$

where S_0 is the $b = 0$ s/mm^2 signal with no diffusion gradient applied. Signal attenuation when combining b with ADC is calculated for the range of ADC-values found in healthy FGT compared to the b-values used in this study. Isolines of signal attenuation as a function of $\exp(-TE/T2)$ is presented in the range of 40 - 140 ms for both TE and T2. And isolines of $\exp(-b \cdot ADC)$ is calculated for a wide range of ADC-values typically found in healthy FGT. The range of b-values is limited to what is used in this research.

Chapter 4

Results

4.1 Noise correction and estimation of T2 and ADC

4.1.1 Signal to background

In order to experimentally retrieve a noise correcting factor NCF a phantom scan was performed while forcing the signal to reach a noise floor. NCF is determined experimentally to be $\exp(1.95) \approx 7.03$ as shown in Figure 4.1. The exact value is used for noise correction. It is assumed that the last three measurements constitute pure intrinsic noise, the average value, 1.95 in the semi-log space is used to estimate NCF.

4.1.2 Direct mapping of biomarkers T2 and ADC

Biomarkers are calculated using the corrected signal according to equation (2.29), with NCF = 7.02868 in MATLAB. Transversal relaxation rate T2 is calculated by a non linear least squares fitting for the corrected DWI signal according to equation (2.13). The calculated T2-values based on the fitted curve is shown for all patients in Table 4.1. In Figure 4.2 is an illustration of ROI placement, all ROIs were placed in the right breast and centered in the FGT to accommodate chemical shift artifacts from left to right in the read direction of the image.
Calculated ADC-values in FGT for all three healthy volunteers is shown in Table 4.2. Analytical derivation of ADC for the same population using b_1 = 100 s/mm^2 and b_2 = 700 s/mm^2, excluding $b = 0$ s/mm^2 according to equation (2.26) is shown in Table 4.3. For clarity in Table 4.4 T2, ADC-values by mono exponential fitting ($ADC_{b=0}$) and analytic estimation ($ADC_{b>0}$) is given for all healthy volunteers with standard deviation.

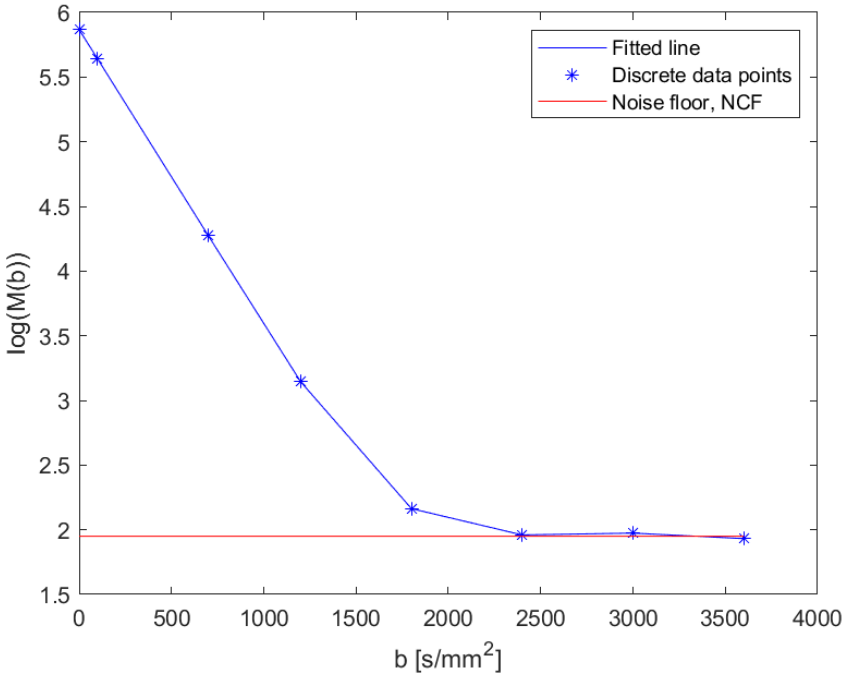

Figure 4.1: Semi-log plot of measured signal $M(b)$ for a Phantom with known diffusion coefficient D. TE = 170 ms, TR = 3600 ms and $b_{\max}$ = 3600 s/mm^2. The noise floor estimate NCF is determined based on the average value of the last three, nearly collinear points.

Table 4.1: Non linear least squares mono exponential fitting of T2 according to equation (2.13).

Subject	$b = 0$ [s/mm^2]	$b = 100$ [s/mm^2]	$b = 700$ [s/mm^2]
1, T2 [ms]	64.40	64.93	71.74
2, T2 [ms]	60.51	62.87	67.86
3, T2 [ms]	50.98	51.60	60.88

Table 4.2: Non linear least squares mono exponential fitting of ADC according to equation (2.25).

Subject	TE = 56 [ms]	TE = 76 [ms]	TE= 96 [ms]	TE = 116 [ms]
1, ADC [mm^2/s]	1.91×10^{-3}	1.95×10^{-3}	1.77×10^{-3}	1.82×10^{-3}
2, ADC [mm^2/s]	1.80×10^{-3}	1.69×10^{-3}	1.66×10^{-3}	1.65×10^{-3}
3, ADC [mm^2/s]	2.06×10^{-3}	1.92×10^{-3}	1.90×10^{-3}	1.80×10^{-3}

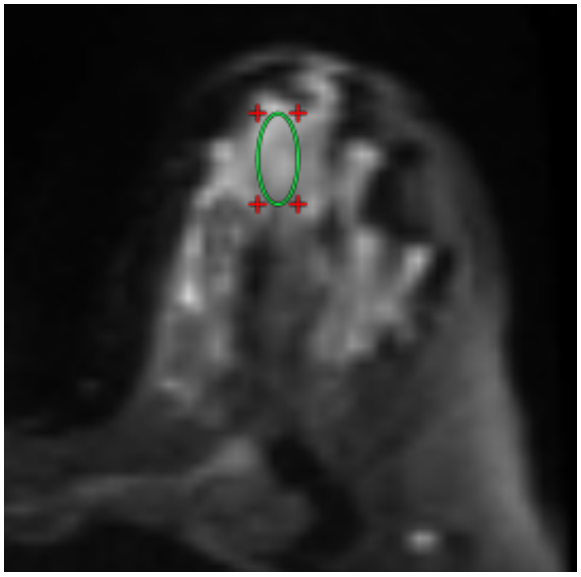

Figure 4.2: Illustration of elliptical ROI in the fibroglandular breast tissue of the right breast in one of the healthy volunteers.

Table 4.3: Analytical estimation of ADC according to equation (2.26), excluding $b = 0$ s/mm^2.

Subject	TE = 56 [ms]	TE = 76 [ms]	TE = 96 [ms]	TE = 116 [ms]
1, ADC [mm^2/s]	1.85×10^{-3}	1.83×10^{-3}	1.70×10^{-3}	1.74×10^{-3}
2, ADC [mm^2/s]	1.72×10^{-3}	1.67×10^{-3}	1.62×10^{-3}	1.62×10^{-3}
3, ADC [mm^2/s]	2.06×10^{-3}	1.88×10^{-3}	1.87×10^{-3}	1.77×10^{-3}

Table 4.4: T2 and ADC for noise corrected data in healthy FGT from DW-MRI, $ADC_{b=0}$ is the non linear least squares fitting result including $b = 0$ s/mm^2, whilst $ADC_{b>0}$ is computed using only two b-values $b > 0$ and is consistently lower compared to ADC estimation including $b = 0$ s/mm^2.

Subject	T2 [ms]	$ADC_{b=0}$ (10^{-3}) [mm^2/s]	$ADC_{b>0}$ (10^{-3}) [mm^2/s]
1	67.02 ±3.35	1.86 ±0.07	1.78 ±0.06
2	63.75 ±3.06	1.79 ±0.05	1.66 ±0.04
3	54.49 ±4.53	1.91 ±0.09	1.89 ±0.10

4.2 Biophysical models

4.2.1 Two compartment model

In the two compartment model the largest extracellular compartment has fixed parameters as noted in section 3.4.1 and the free variable is the intracellular transverse relax-

ation of restricted water, $T2_2$. For easy comparison the experimentally obtained signal and the two compartment modeled signal is plotted in the semi-log space, see Figure 4.3, 4.4 and 4.5. For the bi-exponential model to agree with experimentally obtained measurements the restricted intracellular water is required to have a much higher T2 than that of hindered extracellular water.

The highest prioritized factor for comparing experimental results to the two compartment model is that signal attenuation at high b-values are well approximated, due to observations. In Table 4.5 the numerically computed intracellular $T2_2$ is given for all three healthy volunteers. The mean intracellular T2 is estimated to be $T2_2 = 115 \pm 8.2$ ms.

Table 4.5: Intracellular $T2_2$ computed by best possible fit of two compartment model to experimentally obtained data at b = 100 and 700 s/mm^2 and fixed parameters according to section 3.4.1.

Subject	$T2_2$ [ms]
1	125
2	115
3	105

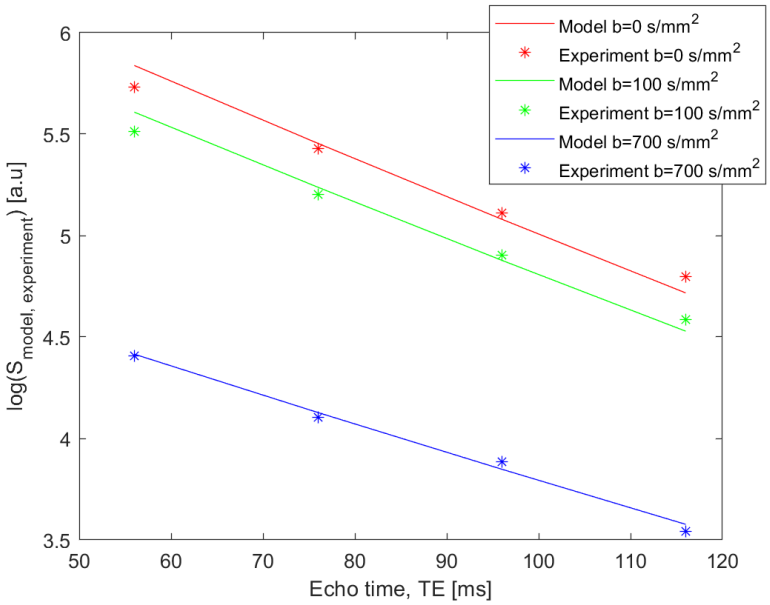

Figure 4.3: Two compartment model (line) compared to experimentally acquired data (stars). Shown in log-space for easy comparison. Experimental data from healthy volunteer 1.

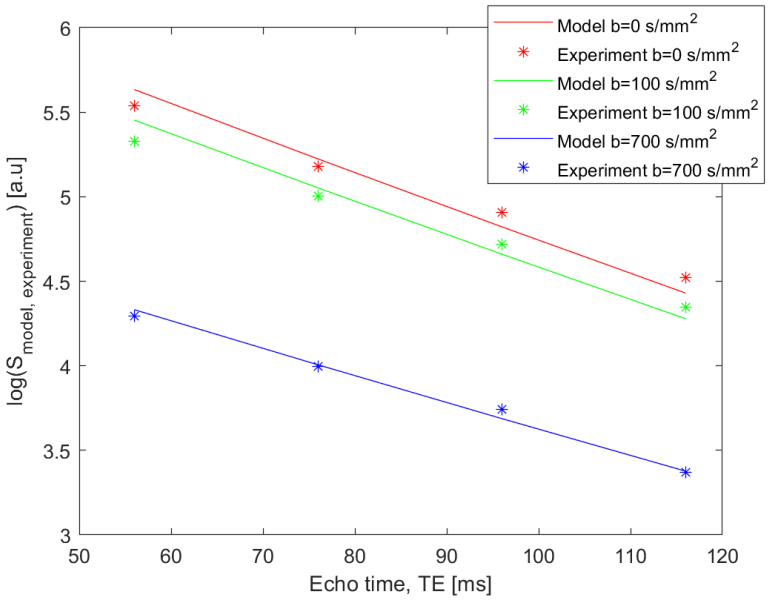

Figure 4.4: Two compartment model (line) compared to experimentally acquired data (stars). Shown in log-space for easy comparison. Experimental data from healthy volunteer 2.

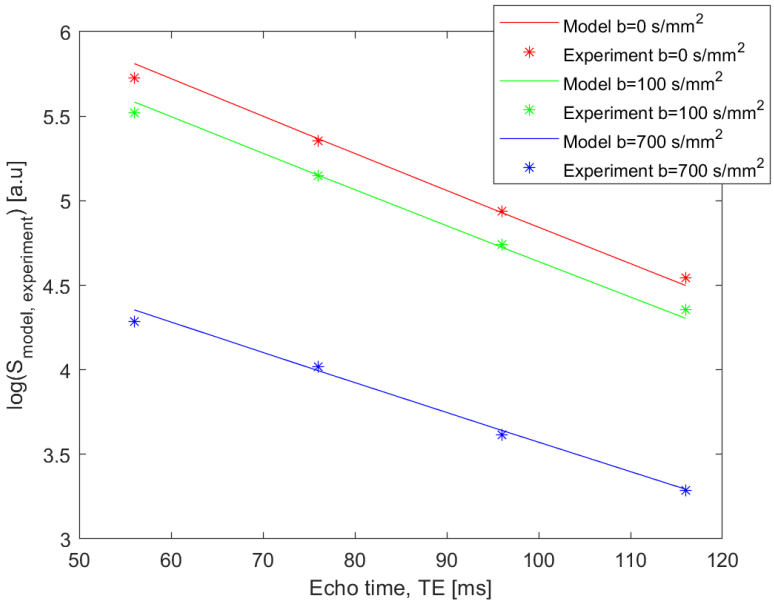

Figure 4.5: Two compartment model (line) compared to experimentally acquired data (stars). Shown in log-space for easy comparison. Experimental data from healthy volunteer 3.

4.2.2 Alternative model

In the alternative model S_0 is the non diffusion weighted signal ($b = 0$ s/mm^2) and the signal S is modeled after the average ADC_{avg} at $b = 100$ and 700 s/mm^2. The general trend in ADC for all volunteers is a decrease for prolonged diffusion time according to TE, both when fitting to a mono exponential model, see Table 4.2 or analytical derivation, Table 4.3. To calculate ADC_{avg} the non linear least squares monoexponential fit with three b-values were used and averaged for all healthy volunteers at each Δ. The average ADC, ADC_{avg} is listed in Table 4.6:

Table 4.6: ADC_{avg} as the average ADC for all healthy volunteers changing according to diffusion time Δ given by protocol parameters listed in Table 3.2.

$\Delta = 24.9$ [ms]	$\Delta = 34.9$ [ms]	$\Delta = 44.9$ [ms]	$\Delta = 54.9$ [ms]
1.87×10^{-3} mm^2/s	1.79×10^{-3} mm^2/s	1.73×10^{-3} mm^2/s	1.71×10^{-3} mm^2/s

Within the measured range the average decrease in ADC_{avg} is estimated by a linear regression of the data in Table 4.6 and presented in Figure 4.6.

4.3 SNR in breast images

A simple signal to noise ratio in DW-MRI images is generated using the experimentally obtained noise correction factor, NCF. Short echo time and low b-values have superior SNR. In Figure 4.7 a contour plot of SNR in the breast images of the patient group is shown. As can be seen, SNR is not for any combination of TE and b below 5 in the DW-MRI, generated from signal within a ROI in FGT.

4.4 Optimization of DW-MRI protocol

Differentiating between signal attenuation due to T2 effects and the application of diffusion sensitizing gradients the isolines of signal attenuation due to $\exp(-TE/T2)$ and $\exp(-b \cdot ADC)$ is presented in Figures 4.8 and 4.9. The theoretically available b-values given the range of TEs used for breast imaging in this research is presented in Figure 4.10. At TE = 116 ms the maximum available b-value was calculated to exceed 18 000 s/mm^2 which is almost twice the capacity of most clinical scanners with an upper limit of typically 10 000 s/mm^2.

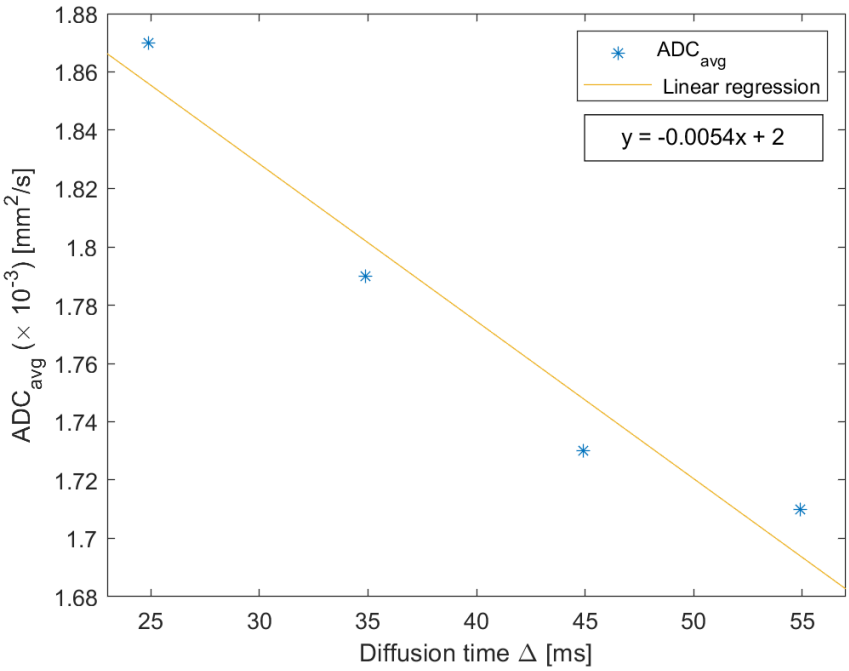

Figure 4.6: Average decrease in ADC as a function of diffusion time Δ. In the interval a linear fit is made, non-linear behaviour is a possibility.

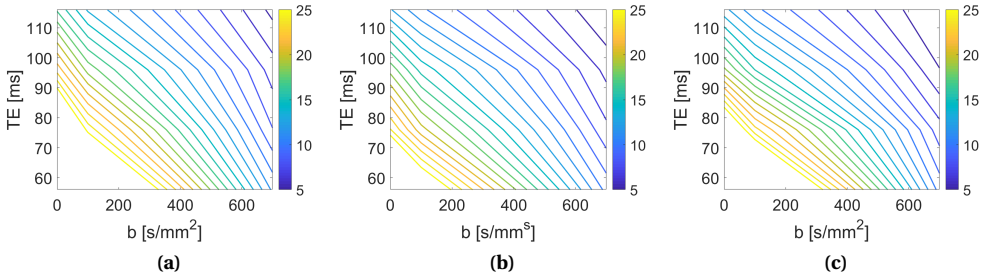

Figure 4.7: a-c shows the contour plot of SNR-values in a ROI in FGT of the right breast for the healthy volunteers 1 through 3.

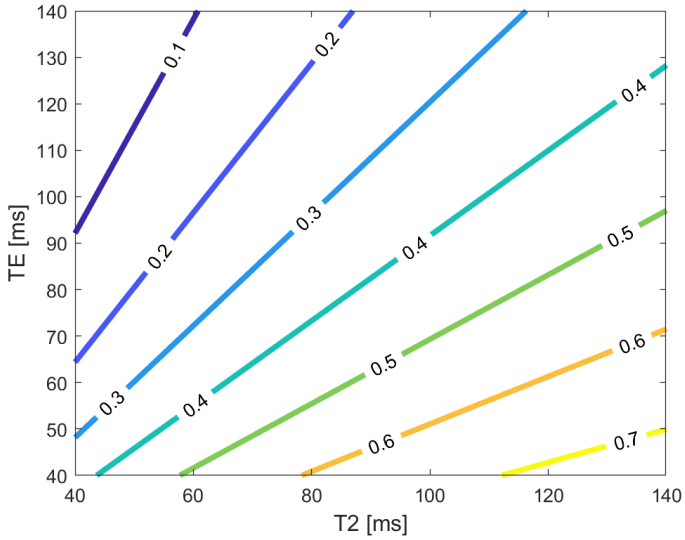

Figure 4.8: Plotted isolines of $\exp(-TE/T2)$ for a range of TE and T2 representing the multiplicative signal attenuation in DW-MRI. Both parameters have a substantial impact on the signal amplitude and therefore on the SNR, regardless of diffusion weighting b.

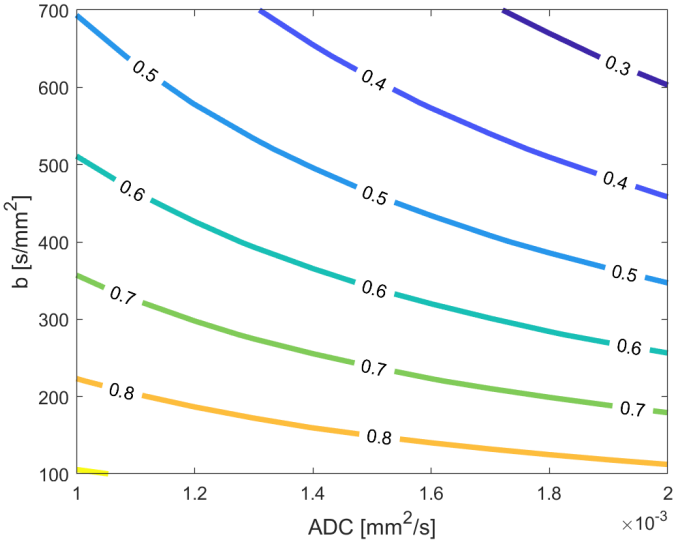

Figure 4.9: Plotted isolines of $\exp(-b \cdot ADC)$ shown for the range of b-values from 0 to 700 s/mm^2, the upper limit used for breast examinations in this study. The ADC range is between 1 and 2 $\times 10^{-3}$ mm^2/s - common values from lesions to healthy tissue.

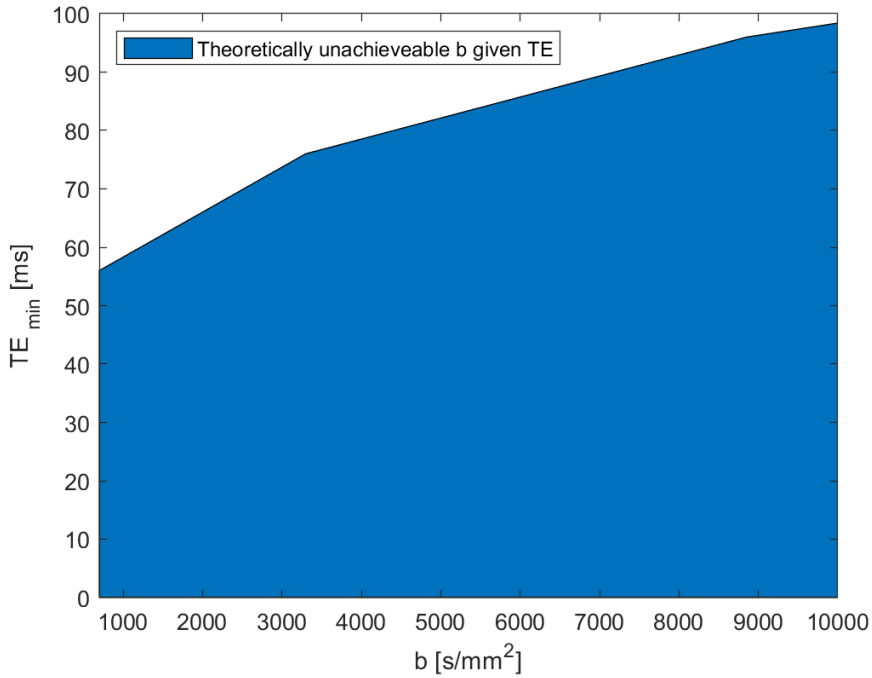

Figure 4.10: Theoretically available regime of b-values according to equation (2.24) given maximum available gradient strength G. Limited to $b = 10\,000$ s/mm^2, typical upper limit on clinical scanners, higher values are theoretically achievable if TE > 100 ms, but is however not practical in a clinical setting due to a near total loss of signal.

Chapter 5

Discussion

5.1 Noise correction

The main source of noise in patient imaging is the body, but the whole measurement chain of the MRI scanner also contributes to the total noise image. Electronics, coils, gradients, Eddy currents and movement all affect the total noise that gives any image a grainy appearance. Longer echo times and higher diffusion weighting leads to lower signal in the image and the signal to noise ratio SNR decreases. For patient imaging and in particular DW-MRI of breasts a high b-value is a two-edged sword, both being more sensitive to diffusion properties in the tissue, but also decreasing SNR. In the diffusion weighted MR images used in this research the SNR is estimated to be sufficiently high causing little to no degrading of image information. Referencing to Figure 4.7 the contour plot of SNR values for the combination of TE and b shows that all retrieveable information from the DW-MRI data is calculated in regions of interest with a SNR of at least 5. For the shortest TE, TE= 56 ms and b = 100 s/mm^2 SNR exceeds 25, which is deemed more than sufficient for extracting information from the image. Nonetheless all data used in this research is corrected for with the intrinsic noise figure NCF according to equation (2.29).

5.2 Direct mapping of biomarkers T2 and ADC

Choosing appropriate ROIs for the calculation of T2 and ADC in FGT were made after checking for any sort of bias in the images. No phase direction bias was found and fat

suppression was deemed sufficient for analysis, chemical shift artifacts were found and accounted for when choosing ROIs. The signal intensity within the ROI was averaged by the software applied. The frequency encoding direction is left to right in the image and a chemical shift can be detected on the left side of each breast as a dark region of signal void due to mismapping of fat and water. Overlapping of signal can be seen on the rightmost side of each breast. ROIs were carefully placed so that overlapping regions were not included.

5.2.1 Direct T2-mapping

T2 is observed to be increasing with diffusion weighting and increases with $b = \gamma^2 G^2 \delta^2 (\Delta - \delta/3)$. It means that the monoexponential behaviour of the signal decay with a given TE is further attenuated with higher diffusion weighting causing an apparent increase in T2. A direct monoexponential mapping shows an increase in T2 from zero diffusion weighting to $b = 700$ s/mm^2 of approximately 8 ms for the group of healthy volunteers as a whole referring to Table 4.1. The reason behind this apparent increase in T2 for diffusion weighted images is suggested to arise from compartmental filtering as theorized in a two compartment model with unique T2-values for each compartment - and is not due to noise or signal loss as the SNR is sufficiently high. In the diffusion weighted images the apparent increase in T2 for increased b-values could be due to a compartmental filtering and a larger weighting from a compartment with longer T2 given by the application of the diffusion gradient G.

5.2.2 Direct ADC-mapping

The observed signal behaviour in a DW-MRI sequence is that T2-mapping is dependent on diffusion weighting. With increase in T2 for increased b one might expect a dependency on TE for the mapping of ADC in the same sequence. ADC is found to be decreasing with increased TE and increased diffusion time Δ. From lowest (TE = 56 ms) to highest (TE = 116 ms) the average ADC for the group decreases with 0.17×10^{-3} mm^2/s. Increasing diffusion time Δ allows the diffusive water molecules in both restricted and hindered environments to perform a random walk over a longer period of time, thus exploring larger portions of their environment. This will in turn be reflected in the ADC and could provide valuable insight as to the composition of cells in the microenvironment. Calculating the mean squared displacement according to equation (2.20) in three dimensions ($n = 3$) for the smallest diffusion time, $\Delta = 24.9$ ms with the average ADC_{avg} at each Δ, compared to the longest diffusion time $\Delta = 54.9$ ms, the av-

erage diffusion length is increasing from 16.7 μm to 23.7 μm. Referring to Figure 2.5 (b) the change in Δ changes the contribution of each compartment to the total ADC, e.g. longer Δ means a lower total ADC due to the lesser contribution from the restricted compartment. The findings of decreased ADC for longer Δ is as expected from theory. In order to make meaningful comparisons across the literature not only the b-values should be indicated, but the timing of the diffusion gradients and the duration of Δ, since different time profiles could lead to different diffusion effects while sharing the same b-value [38]. Water molecules have more time to interact with the microscopic structure of the tissue when long diffusion times are applied leading to a decrease in ADC.

In summary T2 is dependent on the DW-MRI parameter b while ADC is dependent on echo time, TE and the duration of Δ. For a combination of both parameters SNR decreases as shown in Figure 4.7 however it is deemed high enough for all images to not degrade the information extracting capability to any large extent. SNR is at all times at least 5.

5.3 HES stained biopsies of FGT

A natural question to ask is, how does the calculated diffusion length compare to the typical cell diameter in FGT? TruongVo et. al., 2017 reports a mean cell diameter in breast epithelial cells of $11.2 \pm 2.4\,\mu$m [39]. Comparing to the biopsy sample of healthy breast tissue shown in section 2.6 the cells are measured to be in the region of $11 \pm 1\mu$m in diameter, measured with ImageJ [40] using a known pixel size of $0.3447\,\mu$m and measuring manually for a small number of cells ($n = 20$). This means that the majority of the diffusive water molecules that are observed in the DW images come from the largest extracellular compartment since the diffusion lengths that range from roughly 17-24 μm are larger than the cell diameter.

The HES stained sample shown in Figure 5.1 is part of an ongoing doctoral research project by Liv Egnell - supervisor Pål Erik Goa reports a fraction of 15% purple cell clusters (hematoxylin) to 85% other types of tissue (eosin and saffron), calculated by color segmentation of a large series of HES stained samples of FGT. This is of course not directly related to the extracellular volume fraction that is presumed to be 73% based on Springer et. al., 2014 [33]. Assuming the area of the cells in the HES stained sample is the projection of a spherical cell and the total area of the projected spheres sum up to 15%. If the sample is a slab with dimensions x, y and height z equal to twice the radii of

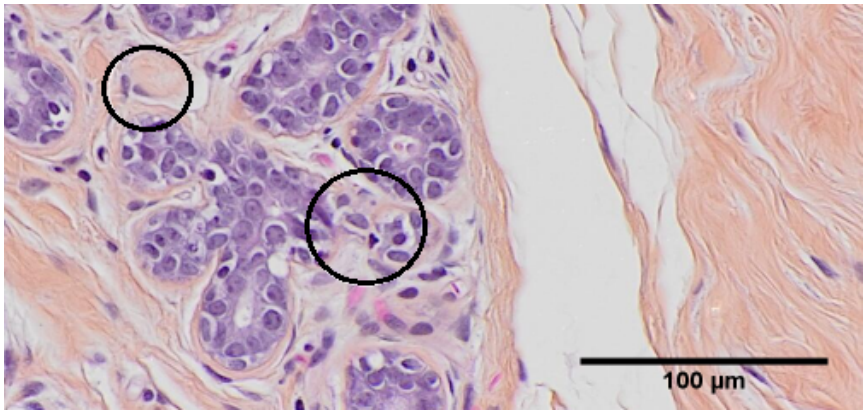

Figure 5.1: A HES stained biopsy sample of healthy breast tissue, the leftmost circle is the circle with radius equal to the smallest diffusion length 16.7 μm and the right circle represents the longest diffusion length with radius 23.7 μm. The big white void in the picture is either fat (adipose tissue) or a drying crack from sample preparation. This particular image is picked due to large amount of cells (purple), the collagen is swirly - typical for healthy tissue. The pink dots may indicate capillaries.

a cell, with a cell diameter of 11μm. Calculating the extracellular volume fraction based on these assumptions gives a fraction of 90% meaning that if the assumptions are fair, the intracellular volume fraction based on the HES stained samples is only 10%. This is smaller than the figure given by Springer et. al., but is not unreasonable when comparing to the collection of HES stained samples, Figure 5.1 is only a small selection of the available data material.

5.4 Biophysical models

A biophysical model is a mathematical simplification of the physical aspects of that system. In this thesis two models of breast tissue are presented, but the transfer value remains for other tissue types. Two common biomarkers for characterization of neoplastic lesions are T2 and ADC that both have characteristic behaviours. Malignant cancers typically have elevated signal in DW-MRI due to reduced ADC, increased water content also gives rise to a change in T2, highlighting lesions in a T2-weighted image. Some of the difficulty with a diffusion weighted image is that the signal is affected by T2-effects and diffusion simultaneously. One of several weaknesses with a biophysical model compared to reality is that assumptions need to be made when translating a real phenomenon into something that is possible to simulate in a useful model - without it being overly complex. Any and every conclusions made based upon a model is affected

by the chosen assumptions, for instance blood flow or *perfusion* is neglected as a source of signal loss in the two compartment model and no membrane flow is accounted for.

5.4.1 Two compartment model

In a two compartment model the assumption is that signal occurs in two regions within the ROI that is measured a signal from. Although the physical processes that creates signal in MRI are well understood, the true origin of signal within complex tissue is less trivial. For simplicity the two compartment model only accounts for water molecules inside and outside of cells. The motivation for examining such a model is to explain the observed behaviour of increased T2 with diffusion weighting and suggest a possible explanation of signal origin. The extracellular compartment, with a volume fraction of $f = 0.73$, Springer et. al., 2014 [33] is assumed to be the largest contributor to signal and the two parameters for ADC_1 and $T2_1$ in this compartment is fixed. When comparing the model to experiment, it is found that the intracellular $T2_2$ is required to be roughly twice as long as $T2_1$ when ADC_2 is fixed at 0.2×10^{-3} mm^2/s. The model displays the same behaviour as experimental data for all b-values and attenuates the DW-MRI-signal at the same rate as seen in Figures 4.3, 4.4 and 4.5. It is however important to note that due to the flexibility of a bi-exponential function and the many degrees of freedom in the two compartment model the result is a product of only one of several hypotheses that can be made. The choice of fixed parameters have paramount influence on the interpretation of results. Other parameters could have been investigated and are potential extensions of the work in this thesis.

5.4.2 Alternative model

The alternative model is based upon the observed behaviour of ADC as a function of TE in a DW-MRI protocol. Figure 4.6 shows that the average decrease in ADC for all volunteers is 1.86×10^{-3} mm^2/s to 1.70×10^{-3} mm^2/s when increasing the diffusion time Δ by 30 ms from the lowest, Δ = 24.9 ms. The signal attenuation decreases for lower ADC given constant b, however, increasing Δ simultaneously means increasing TE and the loss in signal amplitude increases due to T2 relaxation that will exhibit a larger contribution to signal decay compared to change in ADC. The diffusion time-dependent change in ADC is interesting as it provides valuable insight in the behaviour of water molecules in the FGT microenvironment. To conclude, both models are possible explanations to the observed behaviour of T2 and ADC in FGT from a DW-MRI protocol.

5.4.3 Possibility of pseudo diffusion and flow (IVIM)

Another possible explanation for the observed signal behaviour in a diffusion weighted image is the concept of intravoxel inchorent motion (IVIM) coined by Le Bihan in the 1980s [38]. IVIM aims to describe the effect of both diffusion and microcirculation effects or *pseudo-diffusion* caused by blood flow within capillaries in the tissue. The most common mathematical model used to describe the model is:

$$s(b) = S_0(fe^{-bD^*} + (1-f)e^{-bD}), \tag{5.1}$$

where S_0 is the signal for $b = 0$, D and D^* is the diffusion coefficient and the pseudo-diffusion coefficient. f is the perfusion fraction, this model is somewhat similar to the two compartment model but does not account for T2, only diffusion. The perfusion fraction f describes the percent of a voxel volume occupied by capillaries. IVIM has grown more popular over the last few years with improvement in hardware and the fact that perfusion imaging can be done without contrast agents at low b-values < 3-500 s/mm^2 [38]. At low b-values the signal attenuation is greater and calculated ADC is thus higher. IVIM has shown great progress in liver and kidney studies, still a greater insight into the concept and a clear understanding of the strengths and limitations of IVIM is required before we can fully garner the benefit of the method in a clinical setting [38]. When including $b = 0$ in the estimation of ADC a higher value is found suggesting a pseudo diffusion effect on the signal. Separating perfusion from diffusion requires high SNR and IVIM is only prominent at low b-values, without contrast agents there is no danger of gadolinium deposits even though most contrast agents are considered safe.

The IVIM parameter for the perfusion fraction f_{perf} can be estimated analytically from a three b value-scheme [41]. When calculating the perfusion fraction the volume of a voxel found to be consisting of capillaries is calculated to be close to 25 %, which is deemed to be greatly overestimated. It is inherently difficult to separate bulk diffusion effects, water diffusion and micro circulation apart from one another. One issue is how to decide the threshold for the b-value above which IVIM effects no longer occurs and can be considered negligible. This value is often thought to be around 2-400 s/mm^2, but may extend to 600 s/mm^2 in the brain and is expected to vary across organs [38].

5.5 Optimization of protocol

There has been an increased interest in DW-MRI for breast screening in the last decade. One of the reasons for the increased popularity is the ability to detect breast cancers and response to treatment without contrast agents. However there is no general consensus on a standardized approach to DWI for breast imaging in a clinical setting - thus data quality varies widely [42].

The three value b-scheme presented in this research with four equally distributed echo times were deemed to provide images of significantly high SNR for estimation of T2 and ADC. Noise correction had little to no impact on the estimated value of T2 and ADC. Since DW-images are T2-weighted images made sensitive to diffusion through the application of a diffusion sensitizing gradient, diagnostic information can be masked by extraneous long T2 signal, more commonly known as T2 shine through [42]. Both T2 and diffusion processes needs to be addressed. Protocol optimization includes appropriate b-value selection, sufficient SNR, adequate fat suppression and a chosen number of averages. DW-MRI typically requires some post processing of signal, e.g. noise correction and consistent methods for choosing ROIs.

When choosing appropriate b-values for a DW-MRI protocol it is beneficial to have some prior knowledge or experience that can imply what ADC-values one might expect in a certain tissue type or organ. A simple method is simply, look it up in a book or find a table of atypical values. A useful rule of thumb is to pick the b-value in such a manner that $b \cdot ADC \approx 1$.

Choosing echo time in a DWI protocol is of course limited by the desired b-values, the minimum possible TE increases with b. Short TEs are preferred over long TEs due to T2-relaxation effects and loss of signal. Knowing the T2 or at least the expected range can also help in predicting SNR. b = 700 s/mm^2 is the highest available b-value at the shortest echo time TE = 56 ms. The effective gradient strength at the lowest possible TE is calculated to be 60.69 mT/m and is higher than the specified gradient strength of the scanner, this is achieved by applying diffusion sensitizing gradients in the three orthogonal directions of the scanner at once increasing the effective G. Increasing TE by only 20 ms compared to the shortest echo time (TE = 56 ms) greatly extends the range of b to 3297 s/mm^2. A small increase in TE greatly improves the available b-values of the same DW-MRI protocol with a monopolar diffusion scheme based on the Stejskal Tanner protocol. As can be seen in Figure 4.10 at TE ≈ 100 ms the theoretically available

b-value is close to 10 000 s/mm^2, more than enough for all clinical purposes.

With a good prediction of the expected range for both T2 and ADC a simple plot of isolines depicting the theorized signal attenuation for $\exp(-TE/T2)$ and $\exp(-b \cdot ADC)$ as shown in Figures 4.8 and 4.9 are quick and easy tools for choosing appropriate echo times TE and b-values in a DW-MRI protocol of any tissue type or organ.

5.6 Objectives and interpretation of findings

Diffusion is a genuine physical process occurring in the body at all times and is unaffected by the means of measurement as opposed to T1 and T2. Rakow et. al. [43] found a significant increase in $T1$ of breast tissue from 0.5 - 3.0 T and a smaller but still significant decrease of T2 from 0.5 - 3.0 T. Diffusion as an intrinsic property is not dependent on the means of measurement in DWI but the sensitivity to diffusion is primarily the diffusion weighting b, and both the strength of b and the duration of TE and Δ can strongly affect the calculated ADC. Diffusion in breast tissue or other types of tissue for that matter is not entirely random. The presence of cell membranes and other obstacles restrict the path of diffusive molecules. This will in turn affect the apparent diffusion coefficient ADC. When diffusion time Δ increases the ADC decreases and this is probably due to the microstructure of the tissue. Restricted molecules will remain inside the cell membrane and will have nowhere to move other than inside the cell, thus the ADC will decrease and eventlually reach zero for long diffusion times Δ. Hindered extracellular water molecules will have a lower ADC compared to freely diffusing unrestricted water, it will eventually converge to a constant value for long Δ. The decrease in ADC is a sum of the signal contribution from both hindered extracellular and restricted intracellular compartments. The extracellular compartment is by far the largest and will thus have the highest impact on the ADC.

As in most DWI protocols an EPI readout is used for speed and to avoid motion artifacts, also to have a high signal to noise ratio. EPI is however prone to chemical shift artifacts and some mismapping of fat and water is detected in the frequency or read direction in the breast images. This was accounted for when choosing ROIs.

T1 and T2 is in general significantly higher in a cyst compared to normal breast tissue [35]. The observations made in this thesis tells us that the T2 value in breast tissue will increase when based on a simple monoexponential mapping for higher b-values.

Measuring T2 for clinical purposes should however be done without diffusion weighting. Cysts or lesions will still be bright in a DW image due to the T2 shine through from the increased water content of a cyst causing an increase in T2. In a cyst the water content is typically larger compared to healthy tissue increasing cell density and restricting extracellular water diffusion reducing ADC. In diagnostic oncology a common feature of many malign lesions is elevated DWI signal caused by reduced ADC in the tumor microenvironment [1]. A reduction in ADC can aid in distinguishing malignant tumors from benign [44]. In this thesis only healthy tissue is examined and reduction in ADC is due to change in diffusion time Δ.

One of the objectives of this thesis was to evaluate the dependency of diffusion weighting on the estimation of T2. The T2-values increases with added diffusion weighting but the physical explanation is unclear, one possible explanation is compartmental filtering as a function of added diffusion gradient G.

A two compartment model describes the experimental signal behaviour but is highly influenced by the fixed parameters and many degrees of freedom. The alternative model is more straight-forward in that it only accounts for the change in ADC when increasing Δ. The decrease in ADC for higher echo times and longer Δ is directly relating to the microstructure of the tissue and the amount of hindered to restricted diffusion present - or extracellular to intracellular water molecules.

When optimizing a DW-MRI protocol it is important to have a sense of the T2 value or better yet, measure it. In this thesis T2 was measured using a spin echo-EPI protocol with four echo times. But a multi echo spin-echo protocol, often referred to as the gold standard for measuring T2 could have been used instead. An argument for not using the multi echo spin-echo protocol is that the scan time is significantly longer and thus less favored for clinical use. Knowing T2 provides great insight to the expected quality of the DW-images and a guide to the number of repetitions required to acchieve the desired SNR. The desired b-value is restricted by the TE, higher b means longer TE due to the finite strength of the diffusion gradient G, while longer TE also reduces SNR. Equal SNR might be acchieved by increasing the number of repetitions but this leads to significantly longer scan times. Theoretical isolines of constant signal attenuation due to both $\exp(-TE/T2)$ and $\exp(-b \cdot ADC)$ are excellent tools for finding the multiplicative signal attenuation compared to the non-diffusion weighted signal S_0 in a DW-MRI protocol.

Chapter 6

Conclusion

DW-MRI is non-invasive and a valuable tool for exploring tissue architecture in both health and disease. Diffusion weighted images are inherently T2 weighted meaning that the effects of relaxation must be considered simultaneous to water self diffusion in tissue. In the fibroglandular tissue of three healthy female volunteers T2 and ADC were measured with a three-b-value protocol including $b = 0$ s/mm^2 and four uniformly spaced TEs. T2 is found to increase with b and ADC is decreasing for longer TE and increased diffusion time Δ. This suggests that T2 is dependent on b while ADC is dependent on TE and Δ. Two potential biophysical models of breast tissue were evaluated, one two-compartment model and one alternative model based on the observed change in ADC. Each model describes and predicts the experimental behaviour for $b \neq 0$ in terms of the non-diffusion weighted signal S_0, but neither represents a breakthrough in describing the intricate relationship between signal and microstructure in DW-MRI.

Exploring the two compartment model to evaluate other intrinsic properties of the tissue are possible starting points for further research. Another interesting approach in exploring the effect of diffusion time on ADC would be to change the duration of Δ when keeping TE constant.

Bibliography

[1] N. S. White and A. M. Dale, "Distinct effects of nuclear volume fraction and cell diameter on high b-value diffusion MRI contrast in tumors", Magnetic Resonance in Medicine **72**, 1435–1443 (2014).

[2] R. W. Brown, Y.-C. N. Cheng, E. M. Haacke, M. R. Thompson, and R. Venkatesan, eds., *Magnetic Resonance Imaging* (John Wiley & Sons Ltd, Chichester, UK, Apr. 2014).

[3] E. L. Hahn, "Nuclear Induction Due to Free Larmor Precession", Physical Review **77**, 297–298 (1950).

[4] E. L. Hahn, "Spin Echoes", Physical Review **80**, 580–594 (1950).

[5] H. Johansen-Berg and T. E. J. Behrens, *Diffusion MRI : from quantitative measurement to in vivo neuroanatomy* (Academic Press, 2014).

[6] P. C. Lauterbur, "Magnetic resonance zeugmatography", Pure and Applied Chemistry **40**, 149–157 (1974).

[7] P. Mansfield and P. K. Grannell, "Diffraction and microscopy in solids and liquids by nmr", Physical Review B **12**, 3618–3634 (1975).

[8] F. Bloch, "Nuclear Induction", Physical Review **70**, 460–474 (1946).

[9] E. L. Hahn, "Spin Echoes", Physical Review **80**, 580–594 (1950).

[10] J. O. Andersen, *Introduction to statistical mechanics* (Fagbokforlaget, Aug. 2011), pp. 6–12.

[11] D. J. Griffith, *Introduction to electrodynamics*, Vol. 4 (Pearson Education, Inc., 2014).

[12] S. Ljunggren, "A simple graphical representation of fourier-based imaging methods", Journal of Magnetic Resonance (1969) **54**, 338–343 (1983).

[13]D. B. Twieg, "The k-trajectory formulation of the NMR imaging process with applications in analysis and synthesis of imaging methods", Medical Physics **10**, 610–621 (1983).

[14]P. Mansfield, A. A. Maudsley, and B. Sc, *Medical imaging by NMR*, tech. rep. (1977), pp. 188–194.

[15]H. Y. Carr and E. M. Purcell, "Effects of Diffusion on Free Precession in Nuclear Magnetic Resonance Experiments", Physical Review **94**, 630–638 (1954).

[16]E. O. Stejskal and J. E. Tanner, "Spin Diffusion Measurements: Spin Echoes in the Presence of a Time-Dependent Field Gradient", The Journal of Chemical Physics **42**, 288–292 (1965).

[17]S. C. Partridge, N. Nissan, H. Rahbar, A. E. Kitsch, and E. E. Sigmund, "Diffusion-weighted breast MRI: Clinical applications and emerging techniques.", Journal of magnetic resonance imaging : JMRI **45**, 337–355 (2017).

[18]E. O. Stejskal and J. E. Tanner, "Spin Diffusion Measurements: Spin Echoes in the Presence of a Time-Dependent Field Gradient", The Journal of Chemical Physics **42**, 288–292 (1965).

[19]R. M. Henkelman, "Measurement of signal intensities in the presence of noise in MR images", Medical Physics **12**, 232–233 (1985).

[20]J. Allisy-Roberts P. Williams, *Farr's physics for medical imaging* (Saunders, 2008), p. 207.

[21]A. den Dekker and J. Sijbers, "Data distributions in magnetic resonance images: A review", Physica Medica **30**, 725–741 (2014).

[22]J. Sijbers, P. Scheunders, N. Bonnet, D. Van Dyck, and E. Raman, "Quantification and improvement of the signal-to-noise ratio in a magnetic resonance image acquisition procedure", Magnetic Resonance Imaging **14**, 1157–1163 (1996).

[23]S. O. Rice, "Mathematical Analysis of Random Noise", Bell System Technical Journal **23**, 282–332 (1944).

[24]A. Ca´rdenas, C. Ca´rdenas-Blanco, C. Tejos, P. Irarrazaval, and I. Cameron, "Noise in Magnitude Magnetic Resonance Images", 10.1002/cmr.a.20124.

[25]C. G. Koay and P. J. Basser, "Analytically exact correction scheme for signal extraction from noisy magnitude MR signals", Journal of Magnetic Resonance **179**, 317–322 (2006).

[26]D. Le Bihan, E. Breton, D. Lallemand, P. Grenier, E. Cabanis, and M. Laval-Jeantet, "MR imaging of intravoxel incoherent motions: application to diffusion and perfusion in neurologic disorders.", Radiology **161**, 401–7 (1986).

[27] C. Lin, C. Rogers, and S. Majidi, "Fat suppression techniques in breast magnetic resonance imaging: a critical comparison and state of the art", Reports in Medical Imaging **8**, 37 (2015).

[28] S. E. Maier, Y. Sun, and R. V. Mulkern, "Diffusion imaging of brain tumors", NMR in Biomedicine **23**, 849–864 (2010).

[29] J. Pfeuffer, U. Flögel, W. Dreher, and D. Leibfritz, "Restricted diffusion and exchange of intracellular water: theoretical modelling and diffusion time dependence of 1H NMR measurements on perfused glial cells.", NMR in biomedicine **11**, 19–31 (1998).

[30] "MAGNETOM Skyra https://www.siemens-healthineers.com/no/magnetic-resonance-imaging/3t-mri-scanner/magnetom-skyra/technical-details [Accessed 12.05.2019].",

[31] *MATLAB and Statistics Toolbox Release R2016b, The MathWorks, Inc., Natick, Massachusetts, United States.* Nov. 2018.

[32] A. Brühschwein, J. Klever, A.-S. Hoffmann, D. Huber, E. Kaufmann, S. Reese, and A. Meyer-Lindenberg, "Free DICOM-Viewers for Veterinary Medicine", Journal of Digital Imaging (2019) 10.1007/s10278-019-00194-3.

[33] C. S. Springer, X. Li, L. A. Tudorica, K. Y. Oh, N. Roy, S. Y.-C. Chui, A. M. Naik, M. L. Holtorf, A. Afzal, W. D. Rooney, and W. Huang, "Intratumor mapping of intracellular water lifetime: metabolic images of breast cancer?", NMR in biomedicine **27**, 760–73 (2014).

[34] C. Sahin and E. Aribal, "The role of apparent diffusion coefficient values in the differential diagnosis of breast lesions in diffusion-weighted MRI", Diagnostic and Interventional Radiology **19**, 457–62 (2013).

[35] R. E. Hendrick, *Breast MRI : fundamentals and technical aspects* (Springer, 2008), p. 251.

[36] F. Fornasa, "Diffusion-weighted Magnetic Resonance Imaging: What Makes Water Run Fast or Slow?", Journal of clinical imaging science **1**, 27 (2011).

[37] G. Y. Cho, L. Moy, S. G. Kim, S. H. Baete, M. Moccaldi, J. S. Babb, D. K. Sodickson, and E. E. Sigmund, "Evaluation of breast cancer using intravoxel incoherent motion (IVIM) histogram analysis: comparison with malignant status, histological subtype, and molecular prognostic factors", European Radiology **26**, 2547–2558 (2016).

[38] M. Iima and D. Le Bihan, "Clinical Intravoxel Incoherent Motion and Diffusion MR Imaging: Past, Present, and Future", Radiology **278**, 13–32 (2016).

[39] T. N. TruongVo, R. M. Kennedy, H. Chen, A. Chen, A. Berndt, M. Agarwal, L. Zhu, H. Nakshatri, J. Wallace, S. Na, H. Yokota, and J. E. Ryu, "Microfluidic channel for characterizing normal and breast cancer cells", Journal of Micromechanics and Microengineering **27**, 035017 (2017).

[40] "ImageJ - Open platform for scientific image analysis",

[41] O. Jalnefjord, M. Andersson, M. Montelius, G. Starck, A.-K. Elf, V. Johanson, J. Svensson, and M. Ljungberg, "Comparison of methods for estimation of the intravoxel incoherent motion (IVIM) diffusion coefficient (D) and perfusion fraction (f)", Magnetic Resonance Materials in Physics, Biology and Medicine **31**, 715–723 (2018).

[42] S. C. Partridge and E. S. McDonald, "Diffusion weighted MRI of the breast: Protocol optimization, guidelines for interpretation, and potential clinical applications", Magnetic resonance imaging clinics of North America **21**, 601 (2013).

[43] R. Rakow, B. Daniel, A. Sawyer-Glover, and G. Glover, *T1 and T2 Measurements of Breast Tissue at 0.5 T, 1.5 T and 3.0 T*, tech. rep. ().

[44] A. Surov, H. J. Meyer, and A. Wienke, "Correlation between apparent diffusion coefficient (ADC) and cellularity is different in several tumors: a meta-analysis.", Oncotarget **8**, 59492–59499 (2017).